



Cite this: *Dalton Trans.*, 2024, **53**, 12814

Received 15th March 2024,  
Accepted 13th June 2024

DOI: 10.1039/d4dt00776j

rsc.li/dalton

## f-Block hydride complexes – synthesis, structure and reactivity

Richard Drummond Turnbull  and Nicola L. Bell  \*

Complexes formed between the heaviest and lightest elements in the periodic table yield the f-block hydrides, a unique class of compounds with wide-ranging utility and interest, from catalysis to light-responsive materials and nuclear waste storage. Recent developments in syntheses and analytics, such as exploiting low-oxidation state metal ions and improvements in X-ray diffraction tools, have transformed our ability to understand, access and manipulate these important species. This perspective brings together insights from binary metal hydrides, with molecular solution phase studies on heteroleptic complexes and gas phase investigations. It aims to provide an overview of how the f-element influences hydride formation, structure and reactivity including the sometimes-surprising power of co-ligands to tune their behaviour towards a variety of applications.

## Introduction

Although the reactivity of lanthanide and actinide metals towards hydrogen gas had been long observed, it was the Manhattan Project in the 1940s which first brought to light the utility and unique subtleties of hydride complexes of the f-elements.<sup>1</sup> Distinct from their substantially more numerous

main group and d-block counterparts, f-block hydrides are characterised by their predominantly ionic nature, high coordination numbers (which favour bridging hydride ligation) and relatively inaccessible redox activity. These properties, coupled with the inherent photophysical, magnetic and, for some, radioactive nature of the metal ions in these complexes, means that f-block hydrides still represent an important and accelerating field of inorganic chemistry.

Solubilised heteroleptic lanthanide hydrides are found to be the key catalytically active species in a range of hydroelementation transformations<sup>2,3</sup> while binary lanthanide

School of Chemistry, University of Glasgow, Glasgow, UK, G12 8QQ.  
E-mail: Nicola.Bell@Glasgow.ac.uk



**Richard Drummond  
Turnbull**

*in the synthesis and stabilisation of highly-reactive compounds, as well as the development of novel tools and methodologies to aid in this pursuit.*

*Richard Drummond Turnbull hails from Durham in the North-East of England and graduated from Newcastle University with an MChem (Hons) in Chemistry in 2018. He obtained his PhD in Inorganic Chemistry from the University of Manchester in 2023, conducted under the supervision of Prof. Stephen T. Liddle, before pursuing postdoctoral research in the Bell Group at the University of Glasgow. His principal research interests are*



**Nicola L. Bell**

*Dr Nicola Bell was awarded her PhD in 2013 from the University of Edinburgh before undertaking an EPSRC Doctoral Prize Fellowship with Prof. Polly Arnold and later Prof. Jason Love studying actinide imido and oxo complexes. A subsequent period at the University of St Andrews saw Nicola investigate copper catalysis before joining the University of Glasgow in 2019 working on Digital Chemistry. In 2023 Nicola began her independent career with an EPSRC Open Fellowship in Digital Inorganic Chemistry at the University of Glasgow. Dr Bell's research interests encompass f-block coordination chemistry, nuclear applications of chemistry and organometallic catalysis.*



hydrides have also been investigated for applications in methanol synthesis,<sup>4</sup> dinitrogen fixation<sup>5</sup> and neodymium magnet recycling.<sup>6</sup> Useful optical properties exhibited by lanthanide oxyhydrides allow them to be widely utilised in light-responsive materials, such as those now-frequently applied to corrective lenses.<sup>7</sup> At the same time, actinide hydrides represent important potential by-products of radiolysis processes occurring during nuclear waste storage and remediation, which must be understood to facilitate safe nuclear waste handling.<sup>8–10</sup> Superhydrides of both the lanthanides and actinides have demonstrated promise as potential room temperature superconductors and as hydrogen storage materials.<sup>11–13</sup> Actinides have also been demonstrated to activate more challenging substrates, such as converting dinitrogen to ammonia;<sup>14</sup> their reactivity is often unique within the periodic table, making them interesting potential reagents and catalysts in their own right.

Despite their importance, f-block hydrides are often overlooked. In catalysis, their presence is implicated in a wide range of processes; however, the utility of lanthanide alkyl pre-catalyst handling, for example, means the true nature of the hydride involved in these processes is opaque—with consequences for the development of these reactions.

In actinide chemistry, much work to date has focussed on the hydrogenation of actinide metals in the solid state to gain insights into nuclear waste remediation processes; however, bridging the gap between these studies and the well-defined academic curiosities, isolated using complex supporting coligands over the past few decades, has been challenging. Despite this, these heteroleptic actinide hydrides provided valuable contributions towards our understanding of the role of f-orbitals in actinide bonding more generally.<sup>15</sup>

In this perspective, we seek to put into context the chemistry of f-block hydrides, including the synthesis, structure and

reactivity of both lanthanide and actinide hydrides. We give an overview of the behaviour of binary hydrides ( $MH_x$ ) of each period such that the structure and synthesis of heteroleptic molecular hydrides finds context. Within each section, we discuss synthetic strategies, solid-state structure and analytical data on the resulting hydrides and their further reactivity. This work follows on from an extensive early review of the field by Ephritikhine in 1997,<sup>16</sup> drawing upon improvements in analytical data (notably X-ray diffraction), novel synthetic strategies and newly discovered reactivity profiles in the ensuing three decades to provide an overview of the now mature field.

## Homoleptic lanthanide hydrides

### Solid phase binary hydrides – structural insights

In the first step of hydrogen's reaction with bulk metallic lanthanides a solid solution is formed, whereby dihydrogen molecules occupy tetrahedral interstitial sites within the  $Ln(0)$  crystal lattice. Specifically, one half of the sites (the second nearest neighbour sites), are occupied by dihydrogen (Fig. 1).<sup>17</sup> This shifts to occupancy of all sites by a single hydride upon formation of  $LnH_2$  (which has the  $CaF_2$  structure;  $La-H = 2.45 \text{ \AA}$ ). Recent work has demonstrated that  $Ln$  dihydrides ( $Ln = La, Ce$ ) exist as electrode materials with a  $[Ln^{III}(H_t)_2(e^-)]$  formulation.<sup>18</sup> Further hydrogens occupy octahedral sites but defects mean octahedral sites ( $H_o$ ) can start filling before tetrahedral sites ( $H_t$ ) are full. Transformation from  $LnH_2$  to  $LnH_3$  is accompanied by a transition from metal-like to insulating behaviour as the valence electrons are occupied in bonding, with the structure adopting a cubic  $BiF_3$  or trigonal  $HoH_3$  type lattice depending upon cation size ( $La-H_t = 2.43 \text{ \AA}$ ;  $La-H_o = 2.81 \text{ \AA}$ ). At the same time, a transition in optical properties

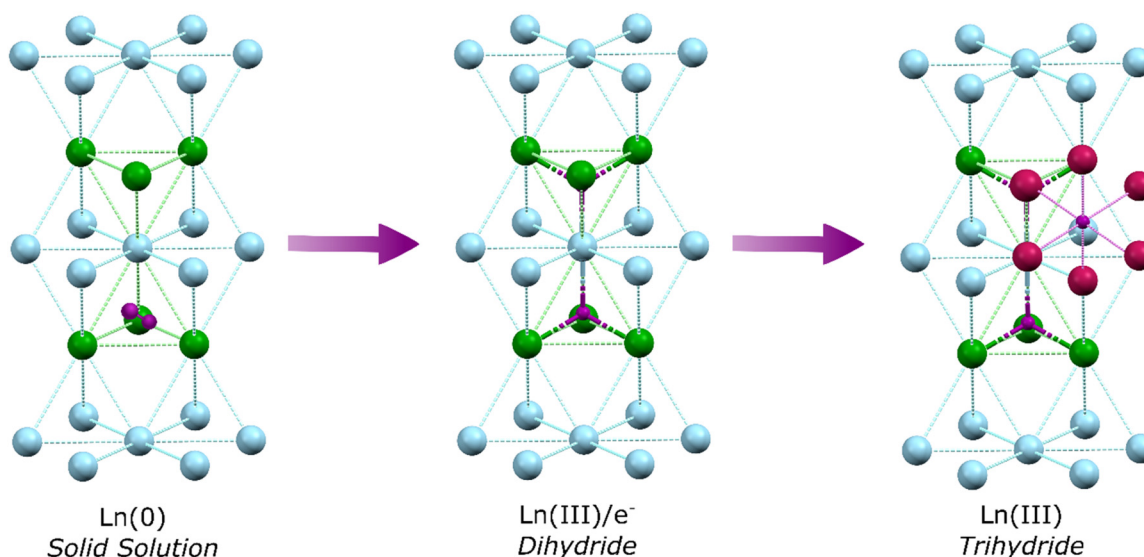


**Fig. 1** The formation of binary lanthanide hydrides from  $Ln(0)$  proceeds via a solid solution, with dihydrogen occupying nearest neighbour sites before oxidation first to lanthanide dihydride, with occupancy of tetrahedral vacancies, then  $Ln^{III}$ , through occupancy of octahedral sites with hydride.  $Ln$  ions: Blue (general), Green (tetrahedral site) or Pink (octahedral site) spheres. Hydrogen/hydride atoms: Purple spheres.



from darkly coloured  $\text{LnH}_2$  to metallic  $\text{LnH}_3$  occurs.<sup>19,20</sup> However, it should be noted that even at a  $>2.9$  H:Ln ratio, conductivity can be high, with small defects in the lattice occupancy yielding superionic conductivity.<sup>21</sup>

### Gas phase/molecular hydrides

Molecular binary lanthanide hydrides have been accessed using laser ablation of lanthanide metal atoms under  $\text{H}_2$  within noble gas matrices. Andrews used this method to investigate the vibrational spectra across a range of  $\text{LnH}_x$  stoichiometries in the gas phase (*i.e.*, molecular examples), thereby finding evidence for a non-linear structure for  $\text{LaH}_2$  in the gas phase, as well as the formation of the  $\text{H}_2$  adduct ( $\text{H}_2\text{CeH}_2$ ).<sup>22,23</sup> This was further investigated across the series, finding that stable adducts of dihydrogen may form with La, Ce, Pr and Nd.<sup>24</sup> Potential stability is more favourable with softer divalent lanthanides which bind molecular  $\text{H}_2$  more strongly than harder trivalent ions, with hydrogen adduct formation occurring *via* transfer of a 6s electron to the  $\text{H}_2$  molecule, and therefore representing the covalent extreme of lanthanide–hydrogen bonding. The trihydrides were also observed; later calculations determined that  $\text{LnH}_3$  complexes exhibit a pyramidal geometry, due to 5d orbital contributions to the bonding.<sup>15</sup> Thus, whilst bonding in these f-block hydrides is mostly ionic, subtle influences, such as interaction with 5f orbitals for the early actinides or with accessible 4f and 5d orbitals for the lanthanides, can have dramatic effects on structure and reactivity.

### Lanthanide superhydrides

Higher stoichiometries,  $\text{Ln}_{4+x}$ , have been shown to be stable under elevated pressure and temperature regimes and are of interest as next-generation superconductors. This is because in these species hydrogen may exist as metallic  $\text{H}(0)$ .<sup>11</sup> The best-studied of these is  $\text{LnH}_{10}$ , which involves a clathrate-type arrangement of H atoms (32 H per Ln) encapsulating the lanthanide ion. These species can be synthesised above  $10^6$

bar pressure in a diamond anvil cell at high temperatures (1000 K). Raman spectroscopy shows no H–H bands, corresponding to bound diatomic hydrogen, despite the fact that  $\text{LaH}_{10}$  contains the shortest H–H distances other than molecular hydrogen.<sup>12</sup>

## Heteroleptic lanthanide hydrides

### Synthetic strategies

**Hydrogenolysis.** Hydrogenolysis of lanthanide alkyl, allyl or aryl complexes is one of the primary synthetic routes to heteroleptic lanthanide hydrides (Fig. 2a). This method has advantages in its simplicity and the generation of only volatile byproducts from the transformation; however, some hydrogenolysis reactions with larger lanthanides (Ce, Nd, Sm), have been shown to be reversible—even in the solid state—necessitating handling and storage of these species under a hydrogen atmosphere.<sup>25</sup>

Okuda *et al.* report the synthesis of the lutetium complex  $[(\text{Me}_4\text{TACD})\text{Lu}(\text{R})_2]^+$ , which reacts with  $\text{H}_2$  at 1 bar pressure in *thf* (Fig. 3). The dialkyl precursor yields a mixture of a ligand-metallated trihydrido dimer,  $[(\text{L}^*)\text{Lu}(\mu^2\text{-H})_3\text{LuL}]^{2+}$  or  $[(\kappa^5\text{-N},\text{N},\text{N},\text{C}-\text{CH}_2-\text{Me}_3\text{TACD})\text{Lu}](\mu^2\text{-H})_3\{\text{Lu}(\kappa^4\text{-N},\text{N},\text{N},\text{N}-\text{Me}_4\text{TACD})\}]^{2+}$ , and a hydrogenated tetrahydrido dimer,  $[(\text{L})\text{Lu}]_2(\mu^2\text{-H})_4]^{2+}$  or  $[(\kappa^4\text{-N},\text{N},\text{N},\text{N}-\text{Me}_4\text{TACD})\text{Lu}]_2(\mu^2\text{-H})_4]^{2+}$ .<sup>26</sup> Based on this (as well as complementary reactions with silanes), the authors conclude that the metalate is an intermediate in the hydrogenation process. Many of the hydrides reported to date either arise directly from metallated complexes (*e.g.*, with substituted metallocene co-ligands) or utilise ligands which are able to undergo metalation.<sup>27–40</sup> Importantly, a survey of the literature demonstrates that these examples allow for hydrogenation at low pressures of  $\text{H}_2$  (1–4 bar). Lanthanide alkyl complexes of ligands which are not known to metallate (*e.g.*,  $\text{Tp}^{\text{R}}$ ) have only been reported under significantly higher pressures for hydro-

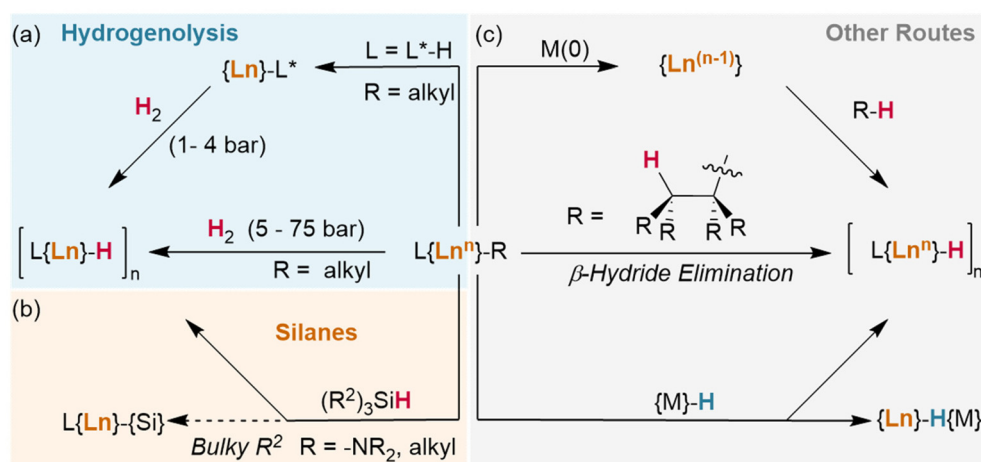


**Fig. 2** Synthetic routes to lanthanide hydrides from  $\text{L}(\text{Ln})-\text{R}$  complexes (a) *via* hydrogenolysis.  $\text{L}^*$  = metallated ligand, accessed via C–H activation/deprotonation. (b) Using silanes. (c) Other routes include reduction with alkali metals,  $\beta$ -hydride elimination and reactions with metal hydrides.



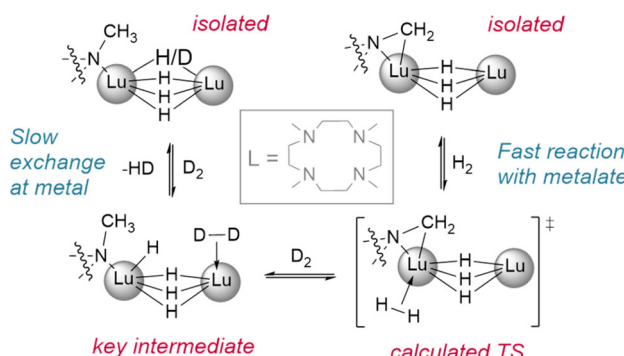


**Fig. 3** Demonstration of the reactivity of metalated ligands in the activation of  $\text{H}_2$ . Deuteration studies show metal based H/D exchange is slow with the tetrahydrido dimer while the metalated trihydrido complex reacts with  $\text{H}_2/\text{D}_2$  quickly.  $\text{L} = \text{Me}_4\text{-TACD}$ .<sup>†</sup>

genolysis (5–75 bar), often with longer reaction times.<sup>41–47</sup> This suggests that the ability of the ligand to metalate provides a significantly lower energy pathway for hydrogenolysis reactions. Kinetic isotope experiments and DFT calculations with these metalated TACD-lutetium hydrides indeed appear to suggest that ligand metalation favours the association of  $\text{H}_2$  before cleaving the M–C bond.

The basicity of the alkyl is also shown to be a key factor for hydrogenolysis. Hou *et al.* demonstrate that hydrogenolysis of the tetrameric methanediide  $\{(\text{Cp}')\text{Lu}\}_4(\mu^2\text{-CH}_2)_4$  ( $\text{Cp}' = \text{C}_5\text{H}_4\text{SiMe}_3$ )<sup>†</sup> yields tetrahedral cluster  $\{(\text{Cp}')\text{Lu}\}_4(\mu^2\text{-Me})_4(\mu^2\text{-H})_2(\mu^3\text{-H})(\mu^4\text{-H})$  through  $\text{H}_2$  addition across the Lu–CH<sub>2</sub> bond.<sup>48</sup> Further hydrogenolysis of the remaining four methyl ligands does not occur in this example. Similarly, treatment of the trimeric cluster  $\{(\text{Cp}')\text{Lu}\}_3(\mu^2\text{-Me})_6$  under the same conditions (1 bar  $\text{H}_2$ , 70 °C) yielded the corresponding tetramer,  $\{(\text{Cp}')\text{Lu}\}_4(\mu^2\text{-Me})_6(\mu^3\text{-Me})(\mu^4\text{-H})$ , where only one of the eight possible methyl groups is protonated off (Fig. 4). This suggests a balance of donor properties, with strongly basic methane ligands competing with hydrides to stabilise the lanthanide complex. At the same time, this work suggests hydride structure persists in solution, at least to a degree sufficient to affect reactivity. These limits are important to understand when considering which lanthanide precatalysts to use in hydrogenation and hydroelementation reactions.

**From silanes.** The safety risks and technical challenges associated with the use of gaseous  $\text{H}_2$  have led some authors to consider alternative hydride sources which are more straightforward

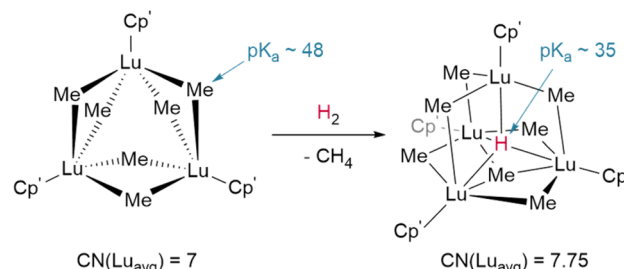


**Fig. 4** Despite the higher  $\text{pK}_a$  of the methyl anion hydrogenolysis occurs with Hou's trimer due to the coordinative stabilisation provided by the  $\mu^4$ -hydride in the tetrameric product. CN = coordination number;  $\text{Cp}' = (\text{C}_5\text{H}_4\text{SiMe}_3)$ .<sup>†</sup>

to handle. Treatment with silanes (*e.g.*,  $\text{PhSiH}_3$ ) is a facile and convenient route to lanthanide hydrides, enabling stoichiometric reactions (which can be challenging with  $\text{H}_2$ ) but reacting similarly in most other ways (Fig. 2b).<sup>26,34,35,49–62</sup>

In an advance on hydrogenolysis reactions, silanes have also been shown to add across  $\text{Ln}-\{\text{N}(\text{SiMe}_3)_2\}$  bonds in addition to lanthanide alkyls,<sup>63,64</sup> and have even been shown to supplant  $\text{Cp}^*$  ( $\text{Cp}^* = \text{C}_5\text{Me}_5$ )<sup>†</sup> as a ligand.<sup>65</sup> However, in rare circumstances, silanes have also been found to participate in other side reactions, including exchange with trimethylsilyl (TMS, Si')<sup>†</sup> groups on  $\text{Ln}-\{\text{CH}_2\text{SiMe}_3\}$  ligands (Fig. 5a/b),<sup>66</sup> although this may be mitigated with ligand steric bulk.<sup>67</sup> In addition, the bulky silane  $\text{H}_2\text{Si}(\text{Si}')_2$  was shown to undergo reversed  $\sigma$ -bond metathesis with  $(\text{Cp}^*)_2\text{Sm}-\text{CH}(\text{Si}')_2$  yielding the  $\text{Ln}-\text{Si}$  product rather than the hydride (Fig. 5c), likely due to steric hindrance preventing the formation of the expected four-centred transition state.<sup>58,69</sup>

Investigating reactions with silanes has also allowed researchers to uncover differences across the lanthanide series, with early lanthanide ( $\text{Me}_3\text{TACD}$ ) $\text{Ln}(\text{allyl})_2$  complexes reacting to give octahydrido tetramer  $\{(\text{Me}_3\text{TACD})\text{Ln}\}_4(\mu^2\text{-H})_8$  while the later lanthanides react with only one equivalent of silane to yield  $\{(\text{Me}_3\text{TACD})\text{Ln}(\text{allyl})\}_2(\mu^2\text{-H})_8$ .<sup>70</sup> This may be due to kinetic rather than thermodynamic factors since the reaction of  $\{(\text{Cp}^*)_2\text{Ln}\}_2(\mu^2\text{-Me})_2$  with  $\text{PhMeSiH}_2$  was found to follow a stepwise mechanism, with a fast initial transformation to  $\{(\text{Cp}^*)_2\text{Ln}\}_2(\mu^2\text{-Me})(\mu^2\text{-H})$  followed by slower hydrogenolysis of the final methyl ligand. The rate of both of these processes decreased across the lanthanide series.<sup>71</sup>

Finally, even the siloxane reagent  $\text{HSi}(\text{OEt})_3$  has been shown to hydrogenate lanthanide complexes (Fig. 6); however, this only occurs from the phenylacetylide bridged dimer  $\{[\eta^5\text{-}\kappa^2\text{-N,N-}(2,5-\{\text{C}(\text{Ph})_2\text{pz}\}-\{\text{N}(\text{Me})\text{pz}\})]\}\text{Yb}(\mu^2\text{-CCPh})_2$  (pz = pyrazole). Reaction with the classical  $\text{Ln}-\text{CH}_2\text{SiMe}_3$  precursor instead yields only the bridged ethoxide analogue  $\{[\eta^5\text{-}\kappa^2\text{-N,N-}(2,5-\{\text{C}(\text{Ph})_2\text{pz}\}-\{\text{N}(\text{Me})\text{pz}\})]\}\text{Yb}(\mu^2\text{-OEt})_2$ . The different bond dissociation energies of the  $\text{Ln}-\text{C}_{\text{sp}}$  vs.  $\text{Ln}-\text{C}_{\text{sp}^3}$  ligands and the ability of the dimer to act cooperatively likely promotes an alternate reaction pathway in the former case.<sup>72</sup>

**Hydride abstraction from alkyls.** It is well-established that  $\text{Ln}-(\text{C}_5\text{H}_5)$  complexes undergo  $\beta$ -hydride elimination reactions;

<sup>†</sup>The following abbreviations will be used throughout this work: Si' =  $-\text{SiMe}_3$ ; N'' =  $\text{N}(\text{SiMe}_3)_2$ ;  $\text{Cp}^* = \text{C}_5(\text{CH}_3)_5$ ;  $\text{Cp}^{**} = \text{C}_5(\text{Ph})_5$ ;  $\text{Cp}^x = \text{C}_5(\text{CH}_3)_4\text{H}$ ;  $\text{Cp}' = \text{C}_5\text{H}_4(\text{SiMe}_3)$ ;  $\text{Cp}'' = 1,3-(\text{SiMe}_3)_2\text{C}_5\text{H}_3$ ;  $\text{Cp}''' = 1,2,4-(\text{SiMe}_3)_3\text{C}_5\text{H}_2$ ;  $\text{Cp}^* = \text{C}_5(\text{CH}_3)_4(\text{SiMe}_3)$ ;  $\text{Cp}^{*\dagger} = \text{C}_5\text{Me}_4(\text{Bu})$ ;  $\text{Cp}^\ddagger = \text{C}_5\text{H}_4(\text{Bu})$ ;  $\text{Cp}^\ddagger = 1,3-(\text{Bu})_2\text{C}_5\text{H}_3$ ;  $\text{Cp}^{*\ddagger} = 1,2,4-(\text{Bu})_3\text{C}_5\text{H}_2$ ;  $\text{Cp}^{\text{An}} = \{3-(\text{SiMe}_3)\text{C}_5\text{H}_4\}_2\text{SiMe}_2$ ;  $\text{Tp}^* = \text{tris}(3,5\text{-dimethylpyrazolyl})$  borane;  $\text{Tp}^{\text{Pr}} = \text{tris}((3\text{-isopropyl-5-methyl)pyrazolyl})$  borane;  $\text{Tp}^{\text{Ad,Me}} = \text{tris}((3\text{-adamantyl-5-methylpyrazolyl})$  borane;  $\text{OSi}^{\text{O}^+} = -\text{OSi}(\text{O}^+\text{Bu})_3$ ;  $(\text{Ad,MeArO})_3\text{mes} = 1,3,5\text{-tris}(\text{methylene}(3\text{-adamantyl-5-methylphenyl-2-ol}))$ mesitylene;  $\text{Me}_4\text{TACD} = 1,4,7,10\text{-tetramethyl-azadodecane}$ .



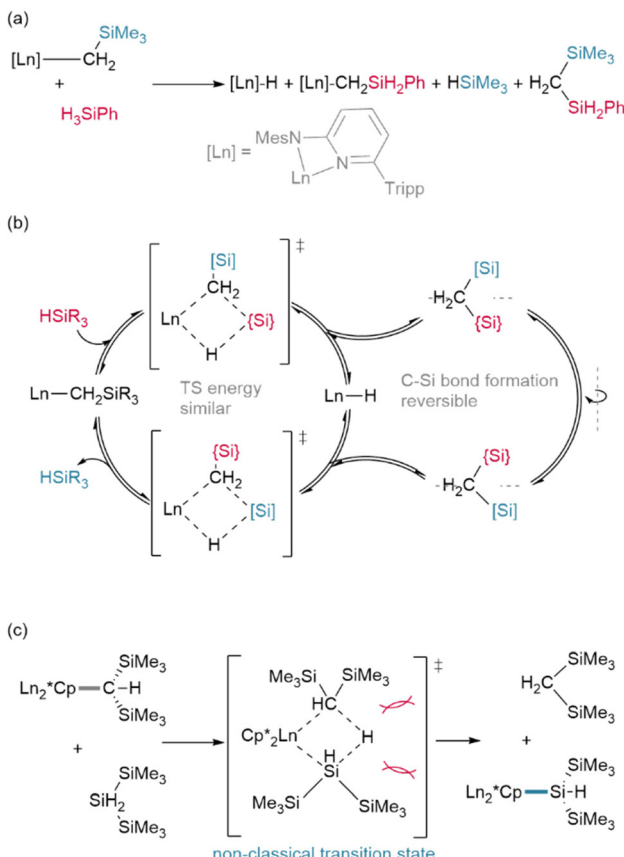


Fig. 5 Alternate non-classical reaction pathways for silanes with lanthanide organometallics: (a) Trifonov *et al.* found a mixture of silyl products from reaction of their  $\text{Ln}-\text{CH}_2\text{SiMe}_3$  complexes with  $\text{PhSiH}_3$  for  $\text{Ln} = \text{Y, Yb}$  (but not  $\text{Lu}$ ) when their ligand was not sufficiently bulky for classical reactivity to occur (Mes = 1,3,5-trimethylphenyl; Tripp = 1,3,5-triisopropylphenyl). (b) A mechanistic explanation for this different behaviour is based upon the reversibility of  $\sigma$ -bond metathesis in these complexes and the similar electronic properties of the  $-\text{[SiMe}_3]$  (blue) and  $-\text{[SiH}_2\text{Ph}}$  (red) groups. Re-attack of the disilylmethane by-product of the reaction in a different orientation can explain all of the products observed. (c) Tilley *et al.* found that bulky silanes reacting with bulky  $\text{Ln}-\text{CH}(\text{SiMe}_3)_2$  ( $\text{Ln} = \text{Sm}$ ) organometallics formed  $\text{Ln}-\text{Si}$  bonds likely due to sterics preventing the formation of a classical 4-membered transition state. Instead the hydride likely occupies the position opposite the lanthanide in the TS for this transformation resulting in C-Si bond formation.

however, this route has been shown to be inferior to hydrogennolysis<sup>73</sup> and, thus, is now a relatively uncommon pathway to hydrides (Fig. 2c). In a rare, recent example of similar behaviour, ethene elimination from the dysprosium methyl trimer  $\{(\text{Cp}^*)\text{Dy}\}_3(\mu^2\text{-Me})_6$  yielded the  $\mu^3$ -hydride product  $\{(\text{Cp}^*)\text{Dy}\}_3(\mu^2\text{-Me})_3(\mu^3\text{-CH}_2)(\mu^3\text{-H})$  (Fig. 7).<sup>74</sup> Cooperative reactivity with triisobutylaluminium reagents was also recently shown to neatly facilitate hydride formation *via* this mechanism.<sup>75,76</sup>

**Using low-valent lanthanides.** Routes to lanthanide(II) complexes have increased dramatically in the past 25 years.<sup>77</sup> Divalent lanthanide precursor reagents, including  $\text{YbI}_2(\text{thf})_2$  and  $\text{EuI}_2(\text{thf})_2$ , have been exploited to access hydride com-

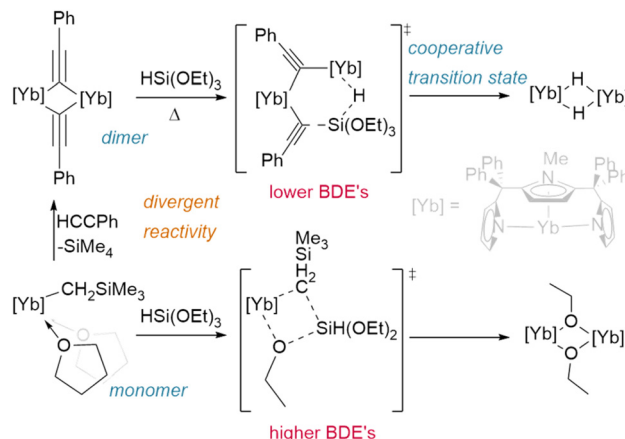


Fig. 6 Divergent reactivity was shown between the monomeric ytterbium alkyl and dimeric ytterbium phenylacetylides upon reaction with  $\text{HSi(OEt)}_3$ , with the dimer proposed to react cooperatively to yield the hydride product.

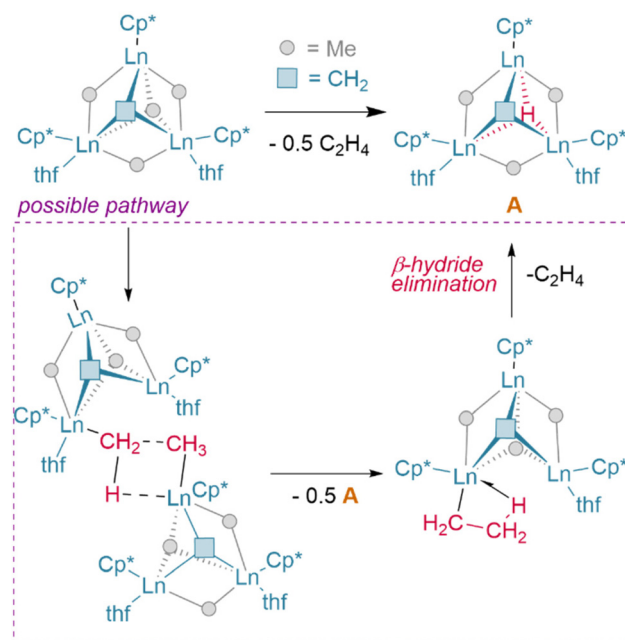


Fig. 7 Spontaneous C=C bond formation from a lanthanide alkyl/alkylidene complex may proceed *via*  $\beta$ -hydride elimination to yield the  $\mu^3$ -hydride product (A).

plexes of these ions.<sup>41,55,78,79</sup> Alternatively, reduction can also provide a route to lanthanide hydride formation from  $\text{Ln}(\text{III})$  (Fig. 2c). Lappert *et al.* observed that treatment of  $\text{Ce}(\text{Cp}^*)_3$  or  $\text{La}(\text{Cp}^*)_3$  ( $\text{Cp}^* = \text{C}_5\text{Me}_4(\text{tBu})\ddagger$ ) with  $\text{K}^0$  in toluene in the presence of 18-crown-6 yielded  $[\text{K}(18\text{-crown-6})][\{(\text{Cp}^*)_3\text{Ln}\}_2(\mu^2\text{-H})]$ , whilst with the bulkier  $\text{Cp}''$  ligand ( $\text{Cp}'' = \text{C}_5\text{H}_3(\text{SiMe}_3)_2$ ) one cyclopentadienyl is lost allowing a reduced toluene dianion to bridge the lanthanide centres.<sup>80</sup> Reduction of a holmium complex with the smaller  $\text{Cp}'$  ligand ( $\text{Cp}' = \text{C}_5\text{H}_4\text{SiMe}_3\ddagger$ ) using lithium naphthalenide,  $\text{Li}(\text{C}_{10}\text{H}_8)$ , in  $\text{Et}_2\text{O}$  yielded a few crys-



tals of  $[\text{Li}(2.2.2\text{-cryptand})]\{(\text{Cp}')_3\text{Ho}\}_2(\mu^2\text{-H})$ ], while the larger terbium analogue gave crystals of the  $\text{Cp}'$  metalate instead (Fig. 8a).<sup>81</sup> Notably, using the same conditions but with lithium metal as a reductant the Tb, Dy and Ho analogues were cleanly reduced to  $\text{Ln}(\text{ii})$  species, suggesting a key role for the reduced arene in hydride formation. Diaconsecu's rationally-prepared  $\{(\text{NN}^{\text{fc}})\text{Lu}(\text{thf})\}_2(\text{C}_{10}\text{H}_8)$  ( $\text{NN}^{\text{fc}} = \kappa^2\text{N},\text{N}[\eta^5\text{-}\{(\text{Me}_2\text{BuSi})\text{N}\}\text{C}_5\text{H}_4\}_2\text{Fe}$ ) was shown to undergo stoichiometric C–H bond activation upon heating, yielding a 1:1 molar ratio

of the corresponding lutetium(III) hydride and naphthalenide  $\{(\text{NN}^{\text{fc}})\text{Lu}(\text{thf})\}_2(\text{C}_{10}\text{H}_7)$  (Fig. 8b).<sup>82</sup> Differential C–H activation behaviour between the lanthanides was also observed with the reduction of lanthanides bound within Meyer's 1,3,5-tris(aryloxo)mesitylene ligand,  $[(\text{Ad},\text{Me}\text{ArO})_3\text{mes}]$ .<sup>†</sup> In this case, reduction with  $\text{KC}_8$  in the presence of crypt in  $\text{thf}/\text{C}_6\text{H}_6$  generated increasing relative yields of a terminal hydride product upon moving from larger to smaller lanthanides, Gd (35%) to Er (45%)—while no hydride was observed under similar conditions for neodymium (Fig. 8c).<sup>83</sup> Hydride formation was suggested to arise from activation at the benzylic position of the reduced central arene (*vide infra*). These data together suggest a key role for reduced arene functions in the formation of  $\text{Ln}-\text{H}$  bonds from  $\text{Ln}(\text{ii})$  complexes, rather than simply *via* abstraction from solvent.

**Lanthanide dihydrogen complexes.** Beyond the gas phase studies discussed above, there is limited, but intriguing, evidence of dihydrogen coordinating a lanthanide centre (as opposed to hydride formation). In 1989,  $(\text{Cp}^*)_2\text{Eu}^{\text{II}}(\eta^2\text{-H}_2)$  was detected by Marks *et al.* using low-temperature NMR studies.<sup>84</sup> The low-valent  $\text{Eu}^{\text{II}}(\text{Cp}^*)_2$  precursor provides an electron-rich centre to stabilise the dihydrogen ligand, with computational studies suggesting the diatom binds in a slightly asymmetric fashion, which can be represented as  $\text{M}^{\delta+}\cdots(\text{H}^{\delta-}\text{-H}^{\delta+})$ .<sup>85</sup>

**Lanthanide hydride structure.** Trimers, tetramers, and hexamers of lanthanide hydrides have all been reported with cluster order increasing as lanthanide coordination number decreases or co-ligand sterics are reduced (Fig. 9). For example, dicationic metal fragments arising from  $\{\text{LM}\}^{2+}$  ( $\text{L}$  = monoanionic ligand;  $\text{M}$  =  $\text{Ln}$ ,  $\text{An}$ ) precursors, such as  $\{\text{CpLn}\}$ , provide higher-order clusters than those arising from monocationic  $\{\text{L}_2\text{M}\}^+$  moieties, such as  $\{\text{Cp}_2\text{Ln}\}$  metallocene complexes.

With dicationic  $\{\text{XM}\}^{2+}$  fragments, small co-ligands such as  $\text{X} = \text{Cp}^*$  and  $\text{Tp}$  ( $\text{Tp}$  = tris(pyrazolyl)borane)<sup>†</sup> can give rise to large hexamers. Few examples exist; however, treatment of  $\text{Ln}(\text{iii})$  complexes  $(\text{Tp})\text{Yb}(\text{CH}_2\text{SiMe}_3)_2$  or  $(\text{Tp})\text{Lu}(\text{CH}_2\text{SiMe}_3)_2$  with  $\text{H}_2$  yields an octahedron of lanthanide ions as a  $\{\text{Ln}_6\text{H}_{12}\}$  cluster with three  $\mu^2$  hydrides, eight face-bridging  $\mu^3$  hydrides, and a single, central  $\mu^6$  ligand—the highest hydride coordination number observed outside of lithium complexes.<sup>86</sup> In contrast, treatment of  $\text{Sm}(\text{ii})$  precursor  $\text{K}[(\text{Cp}^*)_2\text{Sm}^{\text{II}}(\text{CH}_2\text{SiMe}_3)]$  with phenylsilane yields a trigonal prism of oxidised  $\text{Sm}(\text{iii})$  ions, containing a similar central bridging  $\mu^6$  hydride, which is tricapped with potassium ions, yielding a  $\{\text{Sm}_6\text{H}_{15}\}$  core cluster (Fig. 9D).<sup>65</sup>

The slightly larger  $\text{Cp}'^*$  ligand ( $\text{Cp}'^* = \text{C}_5\text{Me}_4(\text{SiMe}_3)$ )<sup>†</sup> yields tetramers<sup>38</sup> with  $\mu^3$  or  $\mu^4$  coordination modes which had been predicted by theory.<sup>87</sup> It should be noted that the  $\mu^6$  and  $\mu^4$  bridging modes of the hydride ligands within lanthanide clusters mirror the ionic binding of hydride in octahedral ( $\text{H}_o$ ) and tetrahedral ( $\text{H}_t$ ) sites, respectively, in the binary lanthanide hydrides (Fig. 1), with indistinguishable bond lengths in the latter case reinforcing the ionic nature of these bonds. In the tetramers, the lanthanides occupy the vertices of a tetrahedron, and the average coordination number of the eight hydrides increases concomitantly with lanthanide ionic

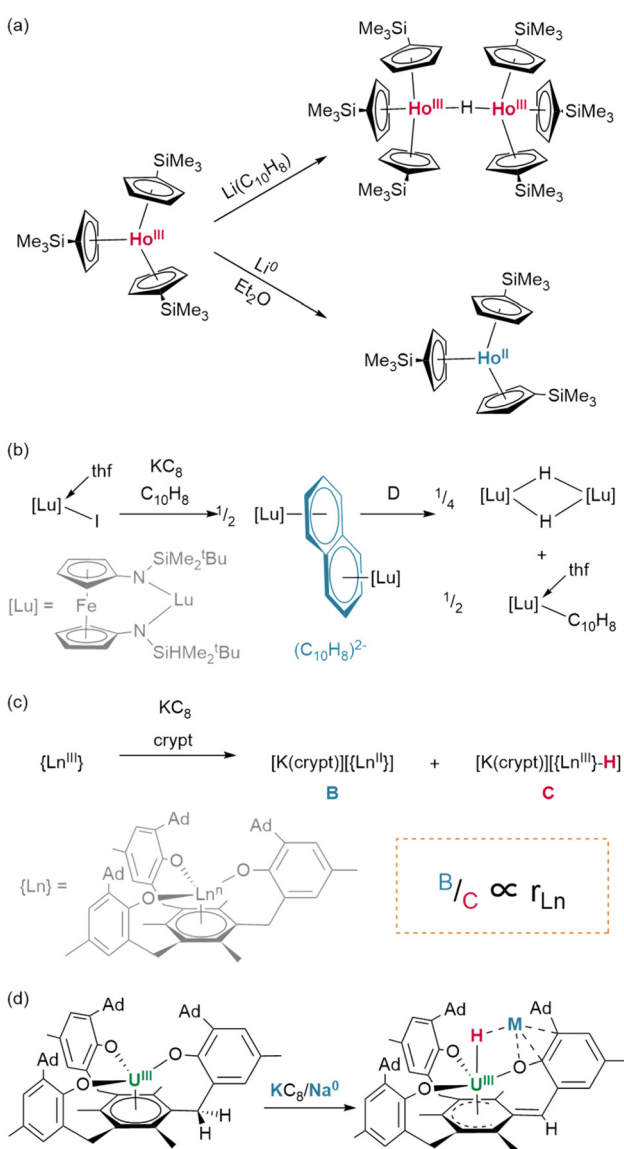


**Fig. 8** Role of arenes in hydride formation under reducing conditions. (a) Hydride formation is observed *via* reduction with lithium naphthalenide but not lithium metal. (b) Diaconsecu's rationally prepared lutetium naphthalenide yields the hydride and a lanthanide aryl cleanly upon heating. (c) Meyer demonstrated the importance of ion size with the ratio of  $\text{Ln}(\text{ii})$  product to lanthanide hydride found to be proportional to metal ionic radius. (d) Lanthanide behaviour can be compared to the uranium reactivity in which the ligand activated species was able to be trapped, demonstrating benzylic C–H activation within this scaffold. crypt = 2,2,2-cryptand.

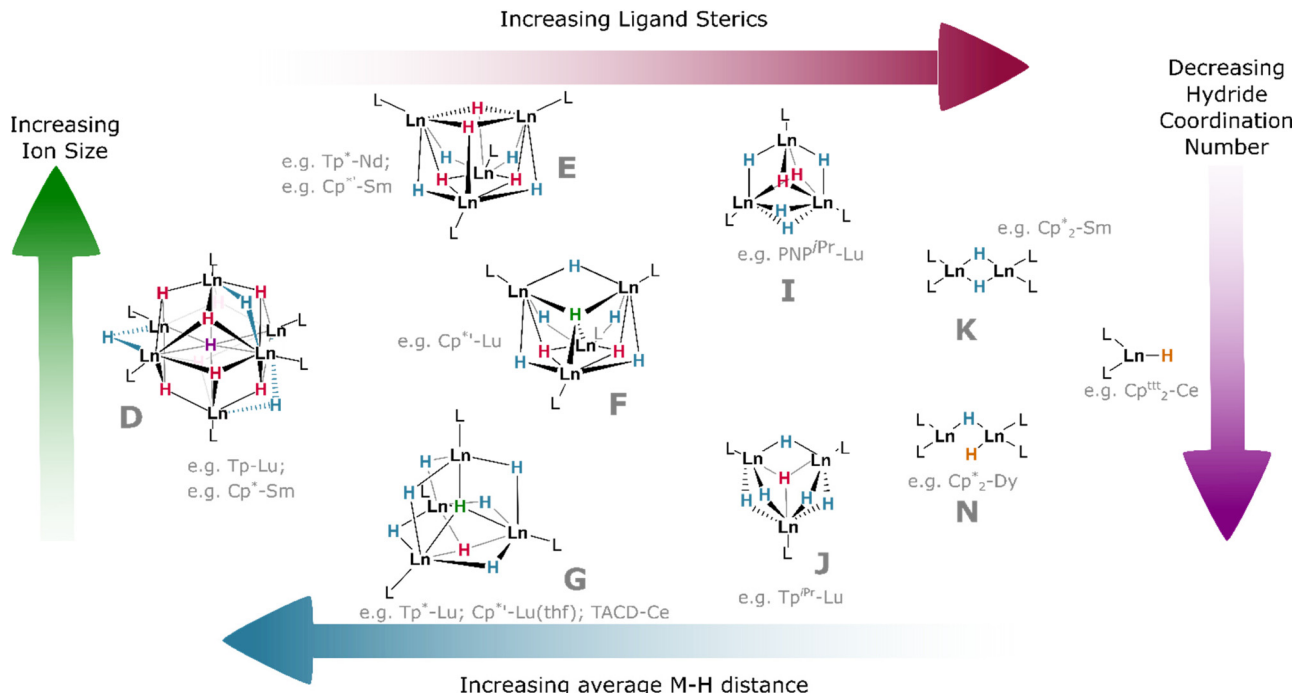


**Fig. 9** Trends in structures of Ln hydride clusters with examples of L and Ln for each set. Ligand abbreviations:  $\text{Cp}^* = \text{C}_5(\text{CH}_3)_5$ ;  $\text{Cp}'^* = \text{C}_5(\text{CH}_3)_4(\text{SiMe}_3)$ ;  $\text{Cp}^{\text{ttt}} = \text{C}_5\text{H}_2(\text{tBu})_3$ ;  $\text{Tp}^* = \text{tris}(3,5\text{-dimethylpyrazolyl})\text{borane}$ ;  $\text{Tp}^{\text{iPr}} = \text{tris}(3\text{-isopropyl-5-methyl})\text{pyrazolyl}\text{borane}$ ;  $\text{PNP}^{\text{iPr}} = \text{N}(\text{o-C}_6\text{H}_4\text{P}(\text{iPr})_2)_2$ ; TACD =  $\kappa^4\text{-N,N,N,N-Me}_4\text{-1,4,7,10-tetraazadodecane}$ .

radius; lutetium complexes, for example, have a greater tendency to include  $\mu^4$  hydrides than the larger lanthanide analogues, with the small  $\{(\text{Cp}'^*)\text{Lu}\}_4(\text{H})_8$  complex comprising one  $\mu^4$ , two  $\mu^3$ , and five  $\mu^2$  hydrides in an overall  $C_{2v}$  symmetric central cluster (Fig. 9F).<sup>58</sup> Complexes of the larger metals yield clusters which have been crystallised as thf solvates:  $\{(\text{Cp}'^*)\text{Nd}\}_4(\text{thf})_2(\text{H})_8$  (and earlier lanthanides) are found with four  $\mu^3$  (2.18–2.34 Å) and four  $\mu^2$  (2.12–2.39 Å) hydrides, with overall  $C_2$  cluster symmetry (Fig. 9E).<sup>38</sup> This trend is also reflected with different co-ligands:  $\{(\text{Tp}^*)\text{Lu}\}_4(\text{H})_8$  ( $\text{Tp}^* = \text{tris}(3,5\text{-dimethylpyrazolyl})\text{borane}$ )<sup>†</sup> incorporates one  $\mu^4$ , one  $\mu^3$ , and six  $\mu^2$  hydrides, giving a  $C_{3v}$ -symmetric cluster (Fig. 9G); while the neodymium example  $\{(\text{Tp}^*)\text{Nd}\}_4(\text{H})_8$  contains one  $\mu^4$  and seven  $\mu^2$  hydrides in a cluster of  $C_{2v}$  symmetry (*cf.* Fig. 9F).<sup>44</sup> That smaller ions tend to construct higher-order bridging interactions is likely due to the contraction of the M–H bonds along the lanthanide series, which declines from 2.40(3) Å/2.26(5) Å ( $\mu^3/\mu^2$ ) in  $\{(\text{Cp}'^*)\text{Pr}\}_4(\text{thf})_2(\text{H})_8$  (Fig. 9E) to 2.13 Å/2.06 Å/2.16 Å ( $\mu^4/\mu^3/\mu^2$ ) in  $\{(\text{Cp}'^*)\text{Lu}\}_4(\text{thf})(\text{H})_8$  (Fig. 9G); indirectly, this is also observed in the concomitant increase in M–H stretching frequency (1307 to 1323 cm<sup>−1</sup>) as the series is progressed. Additionally, the average M···M distance in these clusters spans the range 3.86–3.45 Å (La–Lu). The larger metal ions (La–Sm) retain two solvent molecules per cluster, falling to one at gadolinium, whilst the lutetium example has been characterised as existing without solvent incorporation.<sup>58</sup>

As co-ligand size increases, lower-order clusters become more prevalent. Illustratively, with the  $\text{Tp}^{\text{iPr}}$  ligand ( $\text{Tp}^{\text{iPr}} = \text{tris}(3\text{-isopropyl-5-methyl})\text{pyrazolyl}\text{borane}$ )<sup>†</sup> on Lu(III), a trimer is

formed with one  $\mu^3$  hydride and five  $\mu^2$  hydrides. Bulkier  $\text{Tp}^{\text{tBu,Me}}$  ( $\text{Tp}^{\text{tBu,Me}} = \text{tris}(3\text{-tert-butyl-5-methylpyrazolyl})\text{borane}$ )<sup>†</sup> imposes a dimeric structure to its lower-valent Yb(II) monohydride complex,<sup>45</sup> while the even larger  $\text{Tp}^{\text{Ad,Me}}$  ligand ( $\text{Tp}^{\text{Ad,Me}} = \text{tris}(3\text{-adamantyl-5-methylpyrazolyl})\text{borane}$ )<sup>†</sup> enforces a monomeric structure.<sup>41</sup> The high symmetry of some of these clusters can lead to interesting magnetic properties.<sup>88</sup>

Within the same ligand class, there are identifiable trends in M–H bonding due to clustering. With hexameric  $[(\text{Tp})\text{Lu}(\text{H})_2]_6$ , the average coordination number of the hydrides is 2.8, resulting in a longer M–H bond length of 2.25 Å (2.08–2.48 Å). For the tetrameric analogue with  $\text{Tp}^*$ , the average hydride coordination number falls to 2.4, resulting in a mean M–H length of 2.11 Å (1.87–2.38 Å). Finally, for the trimer resulting from bulky  $\text{Tp}^{\text{iPr}}$ , the average hydride coordination number declines further to 2.2, which gives bond lengths of *ca.* 2.09 Å (1.99–2.25 Å).

In bis(cyclopentadienyl) ‘metallocene’ complexes, lower topology clusters are also favoured, in line with the lower M:H ratio (*vide supra*). Unsubstituted  $\{(\text{Cp})_2\text{La}\}_3(\text{H})_3$  exists as a distorted trimer with two  $\mu^2$  ligands and a single  $\mu^3$  hydride as a result of the large ionic radius of this ion. Whereas  $\text{Cp}'$  complexes of Dy and Tb exist as trimers with three  $\mu^2$  hydrides,  $\text{Cp}'$ -ligated complexes of the same metals exist as dimers;  $[(\text{Cp}^*)_2\text{Dy}(\mu^2\text{-H})]_2$  exhibits one bridging and one terminal hydride, whilst its Tb and Gd analogues exist as  $C_2$ -symmetric dimers with two  $\mu^2$  hydrides. With the very large  $\text{Cp}^*$  ligand, monomeric complexes become isolable across the series: solvated Ce, Dy and Lu examples exhibit bond lengths ranging from 2.27–2.14 Å (Ce–Lu).<sup>25,37</sup>



In ( $\mu^2\text{-H}$ ) species, the lanthanide contraction results in a general decrease in the average M–H bond length across the series (2.38(11) to 2.08(11) Å, La–Lu; see Table 1), and, as the bridging M–H bond length increases, so too does cluster order. Conversely, M–H distance increases upon moving from  $\mu^2$  to  $\mu^3$  bridging modes, then decreases in  $\mu^4$  cases—in the latter case, because the tetrahedral ligand draws the cluster tighter.<sup>89</sup>

**Spectroscopic insights.** IR spectroscopy is also useful in assigning hydride complexes. For the lanthanides, Ln–H vibrations appear around 1100–1300 cm<sup>−1</sup>, but are affected by a variety of factors—including metal identity, ligand sterics, and ligand electronics. Upon moving from  $[(\text{Cp}^*)_2\text{La}(\text{H})]_2$  to  $[(\text{Cp}^*)_2\text{Lu}(\text{H})]_2$ , the IR band for M–H increases from 1120 to 1345 cm<sup>−1</sup> (Table 2), demonstrating the effect of the changes in metal ion; this is likewise reflected in the lower average hydride coordination numbers of later-lanthanide complexes. It is difficult to unpick the precise contributions of ligand sterics, electronics, and clustering to the energies of these vibrations since they are all interrelated; but rare-earth analogues with yttrium can offer some insights: with the difference of a single methyl group,  $\text{Cp}^{\text{Me}}$  dimer  $[(\text{Cp}^{\text{Me}})_2\text{Y}(\text{H})(\text{thf})]_2$  gives rise to a band at 1240 cm<sup>−1</sup>, whereas that of  $[(\text{Cp})_2\text{Y}(\text{H})(\text{thf})]_2$  appears at 1315 cm<sup>−1</sup>. Likewise, that of monomeric  $(\text{Cp}^*)_2\text{Y}(\text{H})(\text{thf})$  appears at 1295 cm<sup>−1</sup>, whilst that of  $[(\text{Cp}^*)\text{Y}(\text{H})]_2$  appears at 1272 cm<sup>−1</sup>. For tetramer  $\{(\text{Cp}^*)\text{Lu}\}_4(\text{H})_8$ , the unsolvated M–H stretch appears at 1304 cm<sup>−1</sup>, differing perceptibly from that of its solvated analogue,  $\{(\text{Cp}^*)\text{Lu}\}_4(\text{H})_8(\text{thf})$ ,

which appears at 1288 cm<sup>−1</sup>. Therefore, reducing the steric bulk of the ligand appears to increase vibrational frequency as the M–H bond lengths shorten. At the same time, the coordination of donor co-ligands (such as solvent) lengthens the M–H bond. As one may expect, increasing cluster order from monomers with terminal bonds to dimers with bridging hydrides has a similar elongating effect, and this is in close concert with bond distances observed by X-ray crystallography.

**Reactivity.** The classical reactivity of Ln–R complexes, including R = H, involves two distinct but related mechanisms:  $\sigma$ -bond metathesis and 1,2-addition reactions (Fig. 10a). Utilizing these modes of reactivity, a wide range of catalytic processes have been developed which involve hydrides as key—but not necessarily isolated—intermediates (Fig. 10b). These reactions usually take advantage of *in situ* reactivity between Ln–R (R = alkyl, amide *etc.*) precatalysts and either silanes or boranes, which generates catalytically-active lanthanide hydrides analogously to stoichiometric processes (*vide infra*). For further insights into lanthanide catalysis from non-hydride precatalysts, we recommend works by Watson, Mindiola, Marks and Eisen.<sup>2,90–92</sup>

**$\sigma$ -Bond metathesis.** Stoichiometric  $\sigma$ -bond metathesis reactions are a staple of lanthanide chemistry, and lanthanide hydrides have been demonstrated to undergo  $\sigma$ -bond metathesis with a wide range of H–E reagents (E = C, N, S, O, P).<sup>16,97</sup> The mechanism proceeds *via* a four-centred transition state, with loss of H<sub>2</sub> gas (Fig. 10).<sup>98</sup>

Amines<sup>45</sup> (E = NR<sub>2</sub>) readily react in this way—and so, too, does ammonia itself (E = NH<sub>2</sub>). However, importantly, the latter was shown to react selectively with the tetrameric cluster  $\{\text{Cp}^*\text{Ln}\}_4(\text{H})_8$ , yielding a heptaammine product which retains the same cluster topology, then undergoes a slower reaction (*ca.* 2 days) with the final, central, tetrahedral  $\mu^4$ -hydride; this seems to demonstrate that hydride structure—which may differ from that of a precatalyst—persists in solution, and that its impact on reactivity can be significant.<sup>99</sup> Ammonium salts (E = NR<sub>3</sub>) have also been used similarly to generate cationic lanthanide fragments.<sup>42</sup>

In another demonstrative case,  $\sigma$ -bond metathesis is mechanistically implicated in catalytic H/D exchange processes which occur between Ln–H centres and certain hydrocarbon substrates (preferentially, those possessed of hydrogens on sp<sup>2</sup>-hybridised carbons, or those with low steric hindrance).<sup>100</sup> Where alternative reaction pathways (insertion/addition; *vide infra*) are also possible, the strong driving force of H<sub>2</sub> loss is a significant factor in favouring  $\sigma$ -bond metathesis; terminal alkynes (E = −C≡CR) most often undergo H–C activation with loss of H<sub>2</sub> to yield Ln–CCR complexes, whereas less acidic alkenes undergo insertion across the Ln–H bond.<sup>54</sup> However, steric effects are also important in determining the reaction outcome: at a sterically-encumbered Yb centre, the disubstituted allene H<sub>2</sub>CCMe<sub>2</sub> preferentially reacts by  $\sigma$ -bond metathesis, whilst less bulky H<sub>2</sub>CCC(H)Cy undergoes 1,2-insertion.<sup>41</sup>

Metathesis of  $\sigma$ -bonds is also the primary process responsible for many ligand activation reactions at lanthanides. As

**Table 1** Average bond lengths (including standard deviation ( $\sigma$ ) for lanthanide hydride clusters in the CSD (including a comparison with the actinide hydrides)

Subset	$\mu^2\text{-M-H}$ (Å)	$\mu^3\text{-M-H}$ (Å)	$\mu^4\text{-M-H}$ (Å)
Dimer	2.17(15)	—	—
Trimer	2.20(20)	2.19(13)	—
Tetramer	2.22(18)	2.36(18)	2.20(12)
Lanthanum	2.38(11)	2.56(14)	2.43(4)
Lutetium	2.08(11)	2.20(14)	2.11(5)
All Lanthanides	2.20(17)	2.29(18)	2.20(12)
All Actinides	2.25(14)	2.35(15)	—

**Table 2** Exemplar rare earth hydride complexes with M–H stretching frequencies. More extensive tables of IR bands for hydrides can be found in ref. 16

Compound	IR Band (cm <sup>−1</sup> )	Assignment	Ref.
Ln–H	1100–1300	M–H	16
$[\text{Cp}^*\text{LaH}]_2$	1120	M–H (bridging)	93
$[\text{Cp}^*\text{LuH}]_2$	1345	M–H (bridging)	93
$[\text{Cp}_2\text{YH}(\text{thf})]_2$	1315	M–H (bridging)	94
$[\text{Cp}^{\text{Me}}_2\text{YH}(\text{thf})]_2$	1240	M–H (bridging)	94
$\text{Cp}^*\text{YH}(\text{thf})$	1295	M–H (terminal)	95
$[\text{Cp}^*\text{YH}]_2$	1272	M–H (bridging)	96
$\{(\text{Cp}^*)\text{Lu}\}_4(\text{H})_8$	1304	M–H (bridging)	58
$\{(\text{Cp}^*)\text{Lu}\}_4(\text{H})_8(\text{thf})$	1288	M–H (bridging)	58



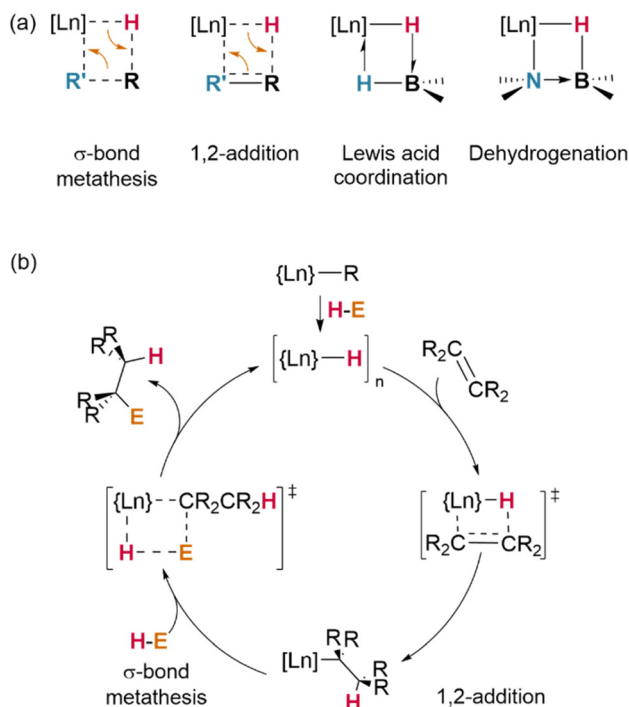


**Fig. 10** Overview of primary mechanisms of reactivity of lanthanide hydrides. (a) Key transition states for primary reaction types. (b) General catalytic scheme for Lanthanide hydride catalysed hydroelementation processes.

demonstrated by Evans and Furche, in  $[(\text{Cp}^*)_2\text{Ln}(\text{H})]_2$ , the activation of  $\text{Cp}^*$  methyl substituents occurs preferentially in complexes of the early (larger) lanthanides—although, in their experiments, a mixture of species was observed in all cases.<sup>28</sup>

Whilst dehalogenation of alkanes by lanthanide hydrides has long been known, Andersen and Maron have more recently demonstrated C–F bond metathesis using a bulky Ce(IV) hydride (Fig. 11).<sup>29</sup> Likewise, dehydrogenative coupling of terminal alkynes with silanes, mediated by a catalytically-active hydride species, is proposed to occur through  $\sigma$ -bond metathesis.<sup>72</sup>

**Addition reactions/insertion reactions.** The primary alternative reactivity profile of these complexes is 1,2-addition, or insertion into the Ln–H bond;<sup>101</sup> this proceeds, mechanistically, through a similar four-centred transition state to  $\sigma$ -bond metathesis (Fig. 10).<sup>102</sup> By this route, insertion of alkenes has been widely utilized for olefin polymerization catalysis,<sup>103</sup>

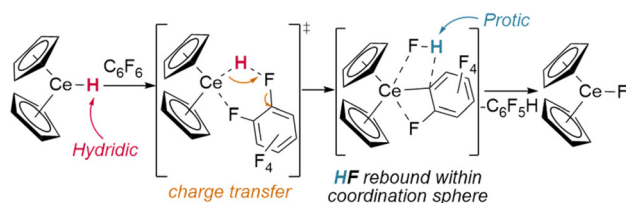


**Fig. 11** Calculated mechanism of  $\text{Ce}^{3+}2\text{CeH}$  reactions with  $\text{C}_6\text{F}_6$  (shown as calculated with  $\text{Cp}$  (i.e.  $\text{C}_5\text{H}_5$ ) for computational simplicity).

while insertion of  $\text{CO}_2$  has been demonstrated to allow copolymerization with epoxides. In stoichiometric reactions, insertion across alkenes,<sup>51</sup> alkynes,<sup>50</sup> ketones,<sup>49</sup> esters,<sup>104</sup> nitriles,<sup>54</sup> isocyanides,<sup>54</sup> and nitrogen heterocycles<sup>49</sup> have all been reported.

Lacking the driving force of  $\text{H}_2$  elimination, the likelihood of alkynes undergoing insertion reactivity over  $\sigma$ -bond metathesis is subject to a fine balance of effects. It has been shown that bis(trimethylsilyl)acetylene undergoes Si–C bond metathesis with  $[(\text{Tp}^{t\text{Bu},\text{Me}})\text{Yb}^{\text{II}}\text{H}]_2$ , yielding the dimer  $[(\text{Tp}^{t\text{Bu},\text{Me}})\text{Yb}^{\text{II}}(\mu^2\text{-}\eta^1\text{-}\eta^2\text{-CCSiMe}_3)]_2$  (Fig. 12)—but bis(trimethylsilyl)but-1,3-diyne instead undergoes an addition reaction to yield a monomeric,  $\eta^3$ -bound product,  $(\text{Tp}^{t\text{Bu},\text{Me}})\text{Yb}^{\text{II}}(\eta^3\text{-Me}_3\text{SiCC-CC(H)SiMe}_3)$ .<sup>45</sup>

Hill and Anker demonstrated that, after olefin insertion into the hydride of  $[(\text{NacNac}^{i\text{Pr}})\text{Yb}^{\text{II}}\text{H}]_2$  ( $\text{NacNac}^{i\text{Pr}} = N,N'$ -bis(diisopropylphenyl)- $\beta$ -pentanedioimide), it is activation of the benzene- $d_6$  solvent which subsequently regenerates the hydride (deuteride) and affords the resultant hydroarylation product (Fig. 13).<sup>63</sup> This reactivity contrasts with classical Ln (III) alkyl activation of benzene, which results in the formation of lanthanide aryl species—and may proceed through a cooperative transition state similar to that proposed by Zhu.<sup>72</sup>

**Dehydrogenation.** In 2013, the catalytic dehydrogenation of dimethylaminoborane was demonstrated to occur through a ligand-assisted process.<sup>105</sup> Initial protonolysis of the hydride yields an amide-tethered borane (Fig. 10a), which can subsequently react to couple  $\text{H}_2\text{B-NMe}_2$  units. Thus, the resting state of the catalyst most likely relies on cooperative lanthanide-borohydride chemistry distinct from Ln–H behaviour.

**Redox reactions.** In recent years, increasing work has been undertaken with low-valent lanthanide complexes with these ions adding a new facet of redox activity to lanthanide behaviour.

Reduction of the *ansa*-cyclopentadienyl ligated dimer  $\{(1\eta^5,1\eta^5\text{-Cp}^{\text{An}})\text{Dy}^{\text{III}}(\text{thf})\}_2(\mu^2\text{-H})_2$  ( $\text{Cp}^{\text{An}} = (\text{Cp}')_2\text{SiMe}_2$ ) resulted

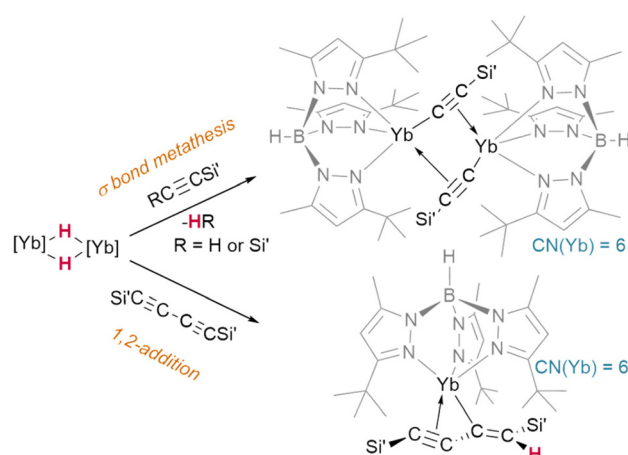


**Fig. 12** Divergent pathways for reactions of ytterbium hydrides with silyl acetylenes ( $[\text{Yb}] = \text{Tp}^{t\text{Bu},\text{Me}}\text{Yb}^{\text{II}}$ ) may be driven by maintaining a high coordination number at the metal.



## Classical reactivity

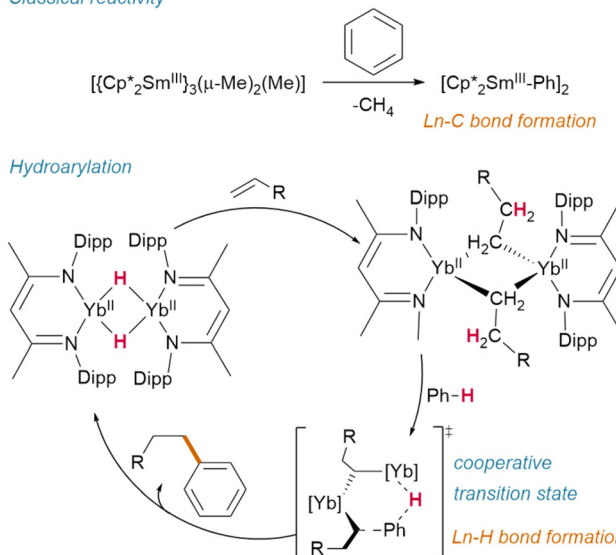


Fig. 13 Hydroarylation catalysed by an ytterbium(II) hydride complex contrasts with classical sigma bond metathesis reactivity observed for Sm(III).

in an unusual ligand rearrangement: in its new, desolvated form,  $[\text{K}(18\text{-crown-6})][\{1\eta^5:2\eta^5\text{-Cp}^{\text{Adm}}\}_2\text{Dy}^{\text{III/II}}_2(\mu^2\text{-H})_2]$ , the supporting ligands bridge between the two metal centres—although it retains the pre-existing  $\{\text{Dy}_2\text{H}_2\}$  core (Fig. 14a).<sup>106</sup>

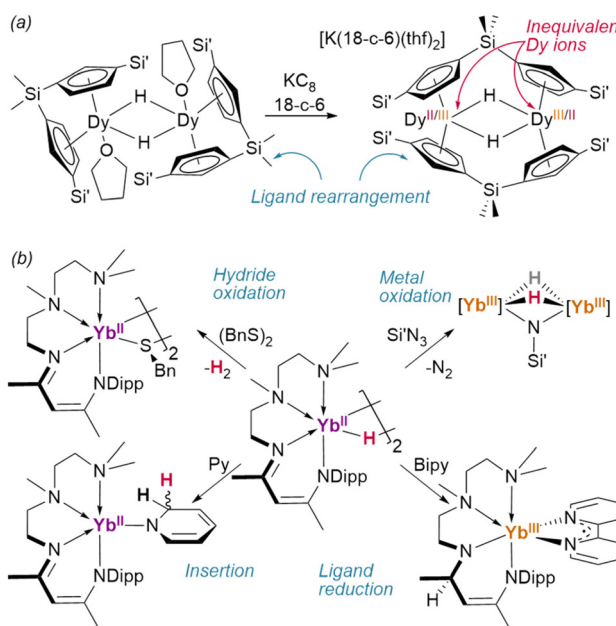


Fig. 14 Redox reactions of lanthanide hydrides. (a) Single electron reduction of the ansa-metallocene ligated dysprosium hydride yields a ligand rearrangement product with unsymmetrical Dy charge density and a calculated Dy–Dy ground state interaction.  $\text{Si}' = \text{SiMe}_3$ ; 18-c-6 = 18-crown-6. (b) Different redox reactivity of a  $\text{Yb}^{\text{II}}$  hydride complex.  $[\text{Yb}] = \{\kappa^4\text{-TMEDA-NacNac}^{\text{Dipp}}\}\text{Yb}$ ; Dipp = 2,6-diisopropylphenyl; Bipy = 2,2'-bipyridine; Py = pyridine.

Intriguingly, low-valent  $\text{Yb}^{\text{II}}$  dihydride  $[\{\kappa^4\text{-TMEDA-NacNac}^{\text{Dipp}}\}\text{Yb}^{\text{II}}(\mu^2\text{-H})_2]$  has been shown to reduce azidotrimethylsilane without perturbing the hydrides, affording a dihydrido-imido  $\text{Yb}^{\text{III}}$  complex (Fig. 14b).<sup>107</sup> In this case, further reaction with  $\text{Se}(0)$  dehydrogenated the complex entirely—while with  $(\text{BnS})_2$  direct dehydrogenation of the hydride was observed to yield the  $\text{Yb}^{\text{III}}$  product.<sup>55</sup> This complex was also shown to reduce 2,2-bipyridine, during which reaction hydride transfer to the NacNac backbone occurs. A  $\text{Tp}^{\text{Ad},\text{iPr}}$  complex of the same ion was also shown to reduce cyclooctatetraene to its dianion, yielding the inverse sandwich product  $\{(\text{Tp}^{\text{Ad},\text{iPr}})\text{Yb}^{\text{III}}\}_2(\text{COT})$  ( $\text{COT} = \text{cyclooctatetraene}$ ).

**Lewis acid coordination.** Worth mentioning is a related mode of reactivity, demonstrated by Evans, in which a Lewis acid (e.g. borane) coordinates to the hydride ligand.<sup>108</sup> This method has also been used to great effect in the synthesis of lanthanide borohydrides and aluminohydrides.

## Lewis acid coordinated lanthanide hydrides

In addition to homometallic clusters of lanthanide hydrides, a wealth of complexes of the form  $\text{Ln}\cdots\text{H-E}$  or  $\text{Ln}\cdots\text{H-M}$  have been reported, ranging from silane complexes containing  $\beta$ -agostic interactions<sup>109,110</sup> (and potentially  $\alpha$ -agostic interaction<sup>111</sup>) to complexes of the  $\text{BH}_4^-$  anion<sup>112</sup> and those of heavier main group and transition metals (Fig. 15).<sup>113,114</sup>

### Borohydrides<sup>108</sup>

Complexes of lanthanides with tetrahydroborate ligands—both  $\text{Ln}^{\text{II}}$  and  $\text{Ln}^{\text{III}}$ —are myriad in the literature,<sup>112</sup> owing in part

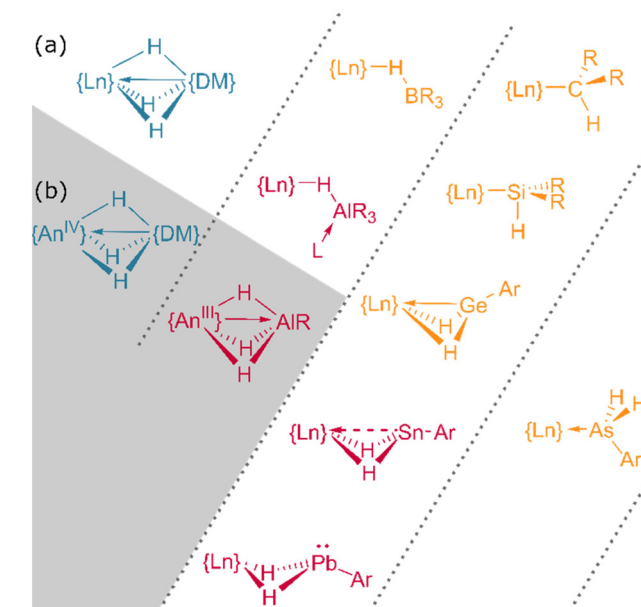


Fig. 15 The bonding interactions of heterobimetallic f-block hydrides. (a) Lanthanide complexes. (b) Actinide complexes. DM = d-block metal. Further examples can be found in ref. 109 and 123.

to the utility of the  $[\text{BH}_4]^-$  anion to act as a pseudohalide in salt metathesis transformations.<sup>115</sup> This borohydride ligand can also adopt multiple coordination modes (terminal,  $\kappa^2$ , and  $\kappa^3$ ), flexibly enabling the synthesis of complexes spanning the lanthanide series. Unlike conventional halides, borohydrides conveniently contain two NMR-active nuclei, discernible IR bands, and are also able to react through protonolysis routes—making these ligands both synthetically and analytically valuable. Borohydride derivatives such as  $[\text{HBR}_3]$ ,<sup>108</sup>  $[\text{HB}(\text{C}_6\text{F}_6)_3]$ ,<sup>116</sup> and tris(pyrazolyl)borane<sup>117</sup> are also able to engage in  $\text{M}\cdots\text{H}\cdots\text{B}$  bridging interactions, stabilising their complexes. The bonding in these complexes is non-intuitive and has been studied in depth concluding that for early transition metals bonding is mostly ionic with some electronic effects modulating the orientation of bridging hydrogens.<sup>118,119</sup>

### Main group hydrides

In contrast to tetrahydroborato ligands ( $[\text{BH}_4]^-$ ), tetrahydroaluminato ligands ( $[\text{AlH}_4]^-$ ) demonstrate a prevalence to bind Lewis bases at the Al(III), generating a 5-coordinate centre upon coordination to a lanthanide and highlighting the ionic nature of the hydride bonding (Fig. 16).<sup>120</sup> In 2013, Anwander *et al.* sought to access homometallic hydrides by treatment of bulky  $\text{Tp}^{\text{tBu},\text{Me}}\text{LuMe}_2$  with two equivalents of  $\text{HALMe}_2$ .<sup>113</sup> Instead, they isolated the ‘masked monomeric dihydride’ insertion product  $\text{Tp}^{\text{tBu},\text{Me}}\text{Lu}(\text{HALMe}_2)_2$ , with a bridging Lu–H–Al interaction ( $\text{Lu–H} = 2.04(3), 2.09(2)$  Å) well within the range for homobimetallic  $\text{TpLn}\cdots\text{H–Ln}$  interactions 1.87–2.09 Å.<sup>113</sup> Similarly, Farnaby and Weetman recently demonstrated the insertion of trihydroaluminium across a  $\{\text{Tp}_2\text{Ln–N}^{\text{H}}\}$  bond, yielding a bridged hydride,  $\text{Tp}_2\text{Ln}(\mu^2\text{H})\text{Al}(\text{H})\text{N}^{\text{H}}$ , with rapidly-exchanging bridging and terminal hydrides.<sup>121</sup> The Anwander group have gone on to expand the scope of  $\text{Ln}\cdots\text{H–E}$  complexes, providing examples with E = Ge, Sn and Pb.<sup>114</sup> In NBO calculations based on their data, they found increasing importance of a direct Ln–E interaction upon moving from Pb to Ge, while the Ln–H bond concurrently lengthens. The bonding, therefore, may be intermediate between that of group 13 and that of group 15 complex  $[\text{Cp}_3\text{Dy–As}(\text{H})_2\text{Mes}]$ , which contains only a Dy–As bond (Fig. 15).<sup>109,122,123</sup>

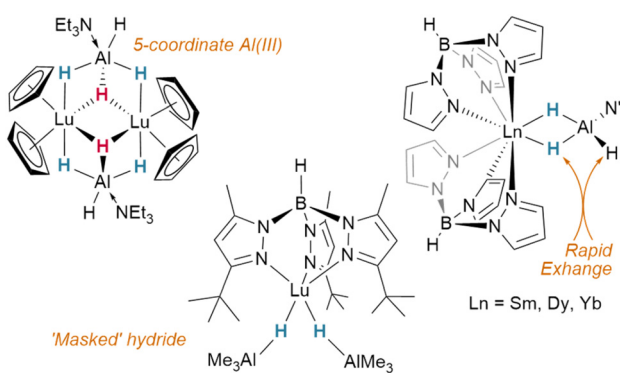


Fig. 16 Examples of aluminohydride complexes of lanthanides.

### Transition metal hydrides

Heterobimetallic complexes with transition metal hydrides have also attracted interest due to the excellent hydrogen storage properties of materials such as  $\text{LaNi}_5\text{H}_x$ . Complexes of lanthanide hydrides with Mo, W, Re, Ru, Os, and Ir are all known and these have been synthesised by a range of routes including alkane elimination,<sup>124</sup> salt elimination,<sup>125</sup> CH activation<sup>126</sup> and  $\text{H}_2$  elimination.<sup>37</sup> Transition metals can lend the lanthanide clusters redox activity which would otherwise be inaccessible, enabling facile C–H bond activation in Cp,  $\text{PPh}_3$  and  $\text{PR}_3$  co-ligands.<sup>126–130</sup> These oxidative addition-like C–H activation steps provide both bridging organometallic and hydride ligands, which buttress direct Ln–TM bonds.<sup>128</sup> In Ln/Mo clusters,  $\text{H}_2$  addition was even observed by single-crystal X-ray diffraction.<sup>131</sup>

### Homoleptic actinide hydrides

The use of the actinides in synthetic chemistry is distinguished from that of the lanthanides in two key respects. First and foremost, the radioactivity of many actinides—particularly the transuranic elements—makes necessary numerous additional precautions and, in the latter case, their handling remains unfeasible in all but the most specialist of laboratory environments; the natural consequence is that markedly less work has been conducted in this area. It is the second respect which makes the effort worthwhile: although their bonding interactions are predominantly electrostatic, the early actinides—especially uranium—are softer, more polarizable metals, for which the valence 5f and 6d orbitals possess sufficient radial extension to impart some degree of covalent character to An–E bonds. As a result, the chemistry of these elements diverges conspicuously from that of the lanthanides—moreover, exhibiting a unique combination of behaviours to which no other region of the periodic table can entirely attest.<sup>132</sup>

### Observations from gas phase and matrix isolation experiments

Early actinide hydrides,  $\text{AnH}_x$  ( $\text{An} = \text{Th, U}; x = 1\text{--}4$ ), have, like their lanthanide analogues, been observed by pulsed laser ablation studies in argon. Under these conditions, where  $x = 1\text{--}3$ , IR spectroscopic measurements indicate that Th–H bonds are somewhat stronger than their uranium analogues—although those of  $\text{UH}_4$  complexes are stronger still.<sup>133,134</sup> Dimeric, hydride-bridged  $\{\text{An}_2\text{H}_2\}$  species are also known for uranium, whereas isostructural thorium analogues have not been observed; calculations imply that a dithorium-bonded  $\{\text{HTh}\equiv\text{ThH}\}$  formulation may be more favourable in this case.<sup>135</sup> Thorium(IV) dihydrogen complexes are also stabilised due to the highly ionic nature of the bonding in  $\text{ThH}_4$  generating polarized  $\text{H}_2$  complexes which exhibit Crabtree’s “dihydrogen bond”-type interactions. This stands in contrast to the uranium example, which has more 5f orbital involvement in bonding. Dihydrogen complexes have also been predicted by these methods and observed in the gas phase and recently in solution (*vide infra*).<sup>136,137</sup>

## Synthesis, isolation and reactivity

Although straightforwardly preparable as a black powder by high-temperature exposure of metallic uranium turnings to H<sub>2</sub> atmosphere (1 bar, up to 250 °C), uranium trihydride (UH<sub>3</sub>) remains a relatively uncommon starting material for the synthesis of molecular uranium complexes.<sup>138–140</sup> The metal initially reacts to generate the metastable  $\alpha$ -UH<sub>3</sub> (orthorhombic) form, which is then transformed into stable  $\beta$ -UH<sub>3</sub> (cubic) at higher temperatures. Somewhat curiously, UH<sub>3</sub> formation is reversible at higher temperatures—a feature which has led actinide materials to be considered for the production and storage of ultrapure hydrogen.<sup>141</sup>

Based on its purportedly superior reactivity, some early reports describe the preferential use of UH<sub>3</sub> over metallic uranium in synthesis;<sup>140</sup> it is presumably its characterisation as intensely pyrophoric which has rather limited the frequency of its applications in the intervening time.<sup>138</sup> That UH<sub>3</sub> can exhibit this particular behaviour is not in doubt; however, the mechanism of its pyrophoricity is not straightforward. By exposure of UH<sub>3</sub> to dry air at elevated temperatures, it has been demonstrated that ignition occurs initially in the gas phase above the metal hydride, consuming H<sub>2</sub> produced in the ensuing reaction and generating sufficient heat to ignite the solid material.<sup>142</sup> Exposure of UH<sub>3</sub> to anoxic water vapour likewise induces oxidation to uranium oxides; however, even at 100 °C, the rate of conversion slows considerably after *ca.* 80% consumption of UH<sub>3</sub>, and temperatures of up to 500 °C are required to achieve complete conversion to U<sub>3</sub>O<sub>8</sub>.<sup>10</sup> A particularly curious complication arises from the work of Hayton and colleagues, whose rationally-synthesised UH<sub>3</sub> powder exhibits essentially no reactivity towards atmospheric gases, and reacts even with aqueous 1 M H<sub>2</sub>SO<sub>4</sub> on the timescale of hours.<sup>143</sup> Such sluggishness has also been apparent in our own investigations of similarly-prepared samples of UH<sub>3</sub>; we are aware of no other precedent for this potent display of lethargy from so reportedly aggressive a reagent. It is plausible that its behaviour depends strongly on its purity and crystalline phase in the solid state; although passivating oxide films have previously been implicated, the preparation of UH<sub>3</sub> as a fine, black powder would necessitate the oxidation of a very considerable surface area, with corresponding impacts on subsequent reaction products and yields, to completely arrest its reactivity. The isolated binary hydride does, of course, undergo reactions with mild oxidants, and under mild reaction conditions yields an array of valuable uranium synthons—including UBr<sub>3</sub>(dme)<sub>2</sub>, UX<sub>4</sub>(dme)<sub>2</sub> (X = Cl, Br, OTf; dme = 1,2-dimethoxyethane), and UI<sub>4</sub>(OEt<sub>2</sub>)<sub>2</sub>.<sup>143,144</sup>

Whilst PaH<sub>3</sub> is known, with forms isostructural to  $\alpha$ - and  $\beta$ -UH<sub>3</sub>, the formulations of other actinide hydrides are broadly different. Two key forms of thorium hydride are known: ThH<sub>2</sub> and Th<sub>4</sub>H<sub>15</sub> (with an H:Th ratio of *ca.* 3.75 : 1). The former is obtained by hydrogenation at 200–350 °C, whilst increased temperatures and H<sub>2</sub> pressures instead yield the higher hydride. Crystalline ThH<sub>2</sub> occurs in the  $I\bar{4}$  space group, wherein the thorium centres are found in an 8-coordinate,

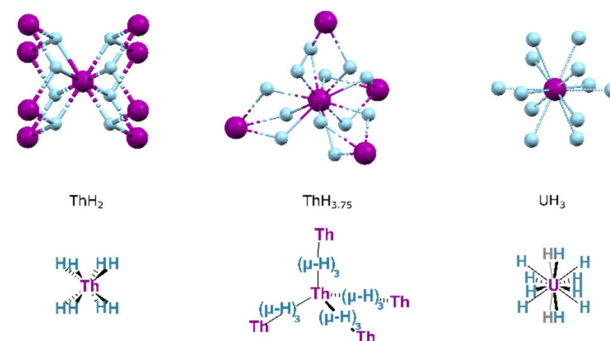


Fig. 17 The local structure of key binary actinide hydrides ThH<sub>2</sub>, Th<sub>4</sub>H<sub>15</sub> and UH<sub>3</sub> illustrating the coordination geometry of the metal in each. Purple Spheres: An ions; Blue Spheres, Hydrides.

square antiprismatic arrangement (Fig. 17). Th<sub>4</sub>H<sub>15</sub> occurs in space group  $I\bar{4}3d$ , in which hydrides adopt a 12-coordinate, cuboctahedral arrangement about each thorium centre. The typical hydrides of the transuranic actinides are AnH<sub>2</sub> formulations, adopting the same fluorite (CaF<sub>2</sub>) structure as their lanthanide congeners, or hexagonal AnH<sub>3</sub> structures.<sup>141</sup>

## Heteroleptic actinide hydrides

A significant portion of the work with heteroleptic actinide hydrides was undertaken as early as the 1980s, and it is conspicuous even amongst other areas of f-block chemistry that the field has developed slowly in the intervening years: only 42 such crystallographically-characterised examples are present in the CSD. Some interest in this area arises from the relatively unusual electronic structures of actinide complexes; in particular, bonding in U, Np and Pu complexes is understood to have the potential to involve some degree of covalency, albeit predominated by ionic character.<sup>145</sup> This raises questions about the nature of An–H bonding, and offers opportunities to consider complexes of these elements in comparison to other actinide elements, as well as to the lanthanides.<sup>145</sup>

## Synthetic routes

**Hydrogenolysis of alkyl complexes.** Much like their lanthanide comparators, the preparation of molecular actinide hydrides is achievable by the hydrogenolysis of An–C bonds in actinide alkyl complexes—indeed, the earliest reported molecular uranium and thorium examples, bimetallic tetrahydrides  $[(Cp^*)_2An(\mu^2\text{-H})(\text{H})]_2$  (An = U, Th), were originally isolated by stoichiometric treatment of toluene solutions of the alkyl precursors, (Cp<sup>\*</sup>)<sub>2</sub>Al(Me)<sub>2</sub> (An = U, Th), with gaseous H<sub>2</sub> (Fig. 18). However, beyond these early examples, the preparation of hydrides by straightforward hydrogenolysis is somewhat less common here than for the lanthanides. In the case of uranium, the range of stable oxidation states available to the metal renders reactivity more complex; whilst the thorium dimer,  $[(Cp^*)_2Th^{\text{IV}}(\mu\text{-H})(\text{H})]_2$ , is stable up to 80 °C,  $[(Cp^*)_2U^{\text{IV}}(\mu\text{-H})(\text{H})]_2$  reductively eliminates H<sub>2</sub> (1 equiv.) upon



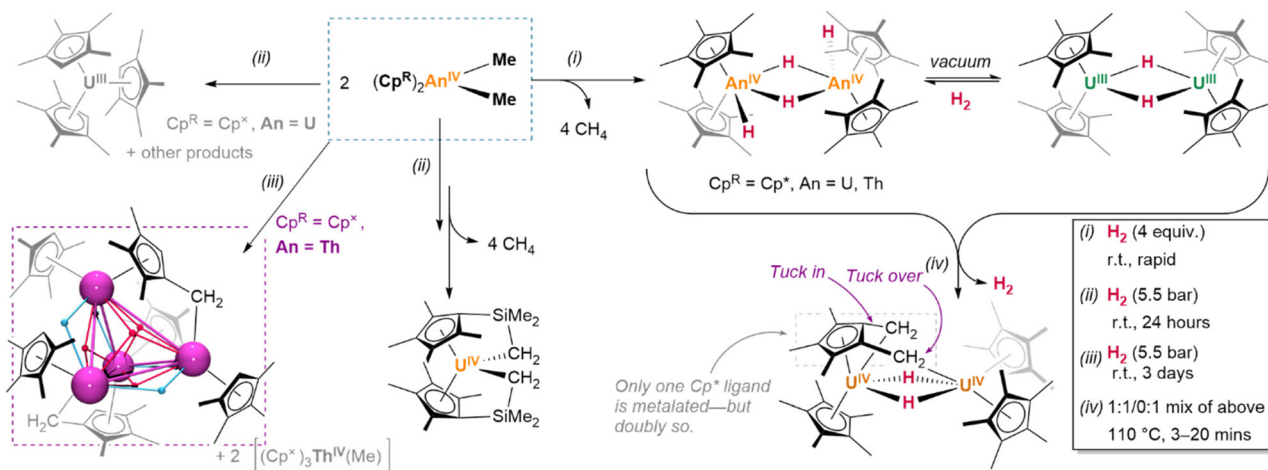


**Fig. 18** Hydrogenolysis of actinide alkyl complexes: thorium complexes tend to form stable hydrides while uranium complexes are able to undergo redox processes which complicate their reactivity. Ligand metalation of the  $\text{Cp}^*$  ligands could arise via similar hydride intermediates observed for the  $\text{Cp}^*$  analogue. Actinide ions: Purple spheres; Bridging hydrides: Blue and red spheres.

standing at ambient temperature,<sup>146</sup> ultimately yielding an isolable bimetallic dihydride,  $[(\text{Cp}^*)_2\text{U}^{\text{III}}(\mu\text{-H})]_2$ .<sup>147</sup> It is notable that when complexes are ligated with substantially bulkier  $\text{Cp}'^*$  ligands, an apparently destabilising effect leads to the exclusive isolation of a  $\text{U}(\text{IV})$  metallacycle.<sup>148</sup> This behaviour is also observed in metalatable  $\text{Cp}^*$  complexes, although the product is instead a ‘tuck-in, tuck-over’ bimetallic hydride complex,  $\{(\text{Cp}^*)_2\text{U}^{\text{IV}}(\mu^2\text{-H})_2\text{U}(\text{Cp}^*)(\text{C}_5\text{Me}_3\text{CH}_2)\}$ ; this is generated upon heating the equilibrium mixture of  $[(\text{Cp}^*)_2\text{U}^{\text{IV}}(\mu^2\text{-H})]_2$  and  $[(\text{Cp}^*)_2\text{U}^{\text{III}}(\mu^2\text{-H})]_2$  to 110 °C.<sup>149</sup>

Despite these considerations (or perhaps because of them), uranium hydrides are frequently accessible under milder hydrogenation conditions than lanthanides (*ca.* 1 bar  $\text{H}_2$ , –40 °C to ambient temperature). For example, diuranium(IV) siloxide complex  $\text{K}_2\{[(\text{Si}^{\text{O}^+}\text{O})_3\text{U}]_2(\mu\text{-O})(\mu\text{-H})_2\}$  ( $\text{Si}^{\text{O}^+}\text{O} = \text{OSi}(\text{O}'\text{Bu})_3$ ), based on a ligand which is not known to metalate, is formed from an oxo-bridged diuranium(III) precursor upon treatment with  $\text{H}_2$  (1 bar, r.t.).<sup>150</sup>

With less accessible redox activity, preparations of thorium hydrides often more closely resemble those of lanthanide congeners; syntheses are somewhat more affected by steric and electronic differences in the coordination sphere of the alkyl precursor complex than the feasibility of ligand cyclometalation. The preparation of a range of thorium hydride clusters,  $[(\text{Cp}^{\text{R}})\text{Th}(\mu^2\text{-H})_3]_n$  ( $n = 5\text{--}13$ , *vide infra*), from thorium monocyclopentadienyl trialkyl precursors, necessitates higher pressures of  $\text{H}_2$  (10–60 bar), elevated temperatures (up to 60 °C), and extended reaction times (12–96 h).<sup>151</sup> Likewise, thorium trialkyl complexes bearing a single, extremely hindered pentaaarylcylopentadienyl ligand undergo a combined protonolysis and hydrogenolysis upon treatment with  $\text{HCp}^*$  or  $\text{HCp}^{\text{x}}$  ( $\text{Cp}^{\text{x}} = \text{C}_5\text{Me}_4\text{H}$ ) and  $\text{H}_2$ , affording the corresponding  $(\text{Cp}^{\text{R}})\text{Th}(\text{H})_2(\text{thf})$  ( $\text{Cp}^{\text{Ar}} = \text{C}_5(3,5\text{-}t\text{-Bu}_2\text{C}_6\text{H}_3)_5$ ,  $\text{Cp}^{\text{R}} = \text{Cp}^*$  or  $\text{Cp}^{\text{x}}$ ) species—although reactions are reported only at relatively high pressures of  $\text{H}_2$  (10–20 bar).<sup>152</sup> Only some preformed thorium bis(cyclopentadienyl) complexes are known to react under

much lower  $\text{H}_2$  pressures; conspicuously, however, this occurs only with supporting ligand systems susceptible to metalation. Representatively, the thorium  $\text{Cp}^*$  complex  $(\text{Cp}^*)_2\text{Th}(\text{Me})_2$  yields a stable tetranuclear octahydride upon exposure to hydrogen gas, in which two of the metallocene methyl substituents are metalated.<sup>148</sup> Considering that greater steric occlusion of the actinide centre in uranium bis(cyclopentadienyl) complexes appears to favour metalation, facilitating facile hydrogenation, the same effect is likely also to be operative here. Conversely, increasing the number of alkyl ligands appears to impede conversion to the hydride; as observed in lanthanide cases, this may be due to the formation of stable, highly-bridged hydride/alkyl intermediates.

**Hydrogenation of nitrides – insights into reversibility.** Whilst hydrogenation conditions need not be forcing, the effective stabilisation of discrete uranium hydrides is highly substrate-dependent. Illustratively, the Mazzanti group’s recent bimetallic  $\text{U}^{\text{III}}/\text{U}^{\text{IV}}$  hydride,  $\{(\text{N}^{\text{v}})_2\text{U}(\text{thf})_2(\mu^2\text{-H})(\mu^2\text{-NH})$ , and mixed-metal  $\text{U}^{\text{IV}}$  species  $\text{Cs}[\{(\text{Si}^{\text{O}^+}\text{O})_3\text{U}\}_2(\mu^2\text{-H})(\mu^2\text{-NH})]$ , are readily prepared by hydrogenation (1 bar, –40 °C) of the respective nitride precursors  $\{(\text{N}^{\text{v}})_2\text{U}(\text{thf})\}_2(\mu^2\text{-N})$  or  $\text{Cs}[\{(\text{Si}^{\text{O}^+}\text{O})_3\text{U}\}_2(\mu^2\text{-N})]$ .<sup>153</sup> However, the former reaction proceeds at –40 °C only with concomitant formation of another cyclometalated complex,  $\{(\text{N}^{\text{v}})_2\text{U}(\text{thf})\}(\mu^2\text{-NH})(\mu^2\text{-}\kappa^2\text{C}_5\text{N}-\text{CH}_2\text{SiMe}_2\text{N}^+)\{\text{U}(\text{N}^{\text{v}})\}$ , which is found present in equal measure with  $\{(\text{N}^{\text{v}})_2\text{U}(\text{thf})\}_2(\mu^2\text{-H})(\mu^2\text{-NH})$ . No reaction is observed at lower temperatures, precluding the arrestation of this further reactivity, and, in the absence of  $\text{H}_2$  atmosphere,  $\text{Cs}[\{(\text{Si}^{\text{O}^+}\text{O})_3\text{U}\}_2(\mu^2\text{-H})(\mu^2\text{-NH})]$  gradually decomposes by loss of  $\text{H}_2$  (*i.e.*, hydrogenation is reversible).<sup>154</sup> Conversely, structurally-related diuranium(IV) complex  $[\text{NBu}_4]\{(\text{Si}^{\text{O}^+}\text{O})_3\text{U}\}_2(\mu^2\text{-NH})(\mu^2\text{-H})$  forms from  $[\text{NBu}_4]\{(\text{Si}^{\text{O}^+}\text{O})_3\text{U}\}_2(\mu^2\text{-N})$  under yet milder conditions of hydrogenation (1 bar, r.t.) and persists even under vacuum.<sup>155</sup> Mazzanti posits that the coordinated alkali metal cation has a destabilising effect on the hydride product, an assertion which is lent weight by catalytic studies with other rare earth hydride

'ate' complexes.<sup>156</sup> It is also interesting to note that complexes of this type were shown to facilitate the reduction of dinitrogen to ammonia by hydrogenolysis.<sup>14</sup>

**Hydride transfer from salts and silanes.** One possible solution to the problem of challenging hydrogenation conditions is the use of alkali metal hydride-transfer reagents, which have been studied somewhat more extensively in actinide systems than in lanthanide congeners. By treatment with NaH, mononuclear  $[\text{Na}(18\text{-crown-6})][\{(\text{Cp}')_3\text{U}(\text{H})\}]$ , dinuclear  $[\text{Na}(18\text{-crown-6})(\text{thf})_2][\{(\text{Cp}')_3\text{U}^{\text{III}}\}_2(\mu^2\text{-H})]$ , and Na-bridged 'ate' complex  $[\text{Na}(\text{thf})_2][\{(\text{Cp}')_3\text{U}^{\text{IV}}\}_2(\mu^2\text{-H})]$  are respectively accessible from the corresponding  $(\text{Cp}')_3\text{U}^{\text{IV}}(\text{Cl})$  or  $(\text{Cp}')_3\text{U}^{\text{III}}(\text{thf})$  (Fig. 19a);<sup>157–159</sup> comparably, in the presence of 2.2.2-cryptand, treatment of *in situ*-generated  $(\text{Cp}')_3\text{U}^{\text{III}}$  with KH affords mononuclear  $[\text{K}(2.2.2\text{-cryptand})][\{(\text{Cp}')_3\text{U}^{\text{III}}(\text{H})\}]$  (Fig. 19a),<sup>160</sup> whilst thorium(IV) tris(cyclopentadienyl) complex  $(\text{Cp}^{\ddagger})_3\text{Th}^{\text{IV}}(\text{Cl})$  ( $\text{Cp}^{\ddagger} = 1,3\text{-}(\text{Bu})_2\text{C}_5\text{H}_3$ ) reacts with excess KH to yield the corresponding monomeric hydride.<sup>161</sup>

Alternatively, but in similar fashion to lanthanide examples, the exchange of An–C for An–H linkages is also achievable by actinide complexes through the  $\sigma$ -bond metathesis of silanes. Complementarily to the original, hydrogenative preparations of  $[(\text{Cp}^*)_2\text{An}(\text{H})_2]_2$  (An = U, Th), Kiplinger and colleagues report that treatment of  $(\text{Cp}^*)_2\text{An}(\text{Me})_2$  with  $\text{PhSiH}_3$  (toluene, 50 °C, 30 minutes) effects the near-quantitative conversion of these alkyl complexes to the respective hydrides.<sup>162</sup> Reactions with  $\text{K}(\text{HBET}_3)$  salts may also generate hydrides with concomitant loss of  $\text{K}(\text{RBET}_3)$ : treatment of tris(cyclopentadienyl) halide precursor  $(\text{Cp}')_3\text{U}^{\text{IV}}\text{Cl}$  with  $\text{K}(\text{HBET}_3)$  effects the abstraction and exchange of chloride for hydride, yielding  $(\text{Cp}')_3\text{U}^{\text{IV}}(\text{H})$  (Fig. 19b).<sup>157</sup>

**Low valent actinides.** Though a relatively new development, low-valent actinide complexes (*i.e.* U(II), Th(II), Th(III)) also offer excellent opportunities to access hydrides. Treatment of divalent  $[\text{K}(18\text{-crown-6})(\text{thf})_2][\{(\text{Cp}')_3\text{Th}^{\text{II}}\}]$  with  $[\text{Et}_3\text{NH}][\text{BPh}_4]$  affords a mixture of trivalent  $(\text{Cp}')_3\text{Th}^{\text{III}}$  and tetravalent  $(\text{Cp}')_3\text{Th}^{\text{IV}}(\text{H})$ . This same Th(II) 'ate' complex also reacts with  $\text{H}_2$  (4 bar, r.t.) in the solid state and in thf solution (1 bar, 0 °C)—although the hydride-containing product is instead the trihydride-bridged dimer  $[\text{K}(18\text{-crown-6})(\text{Et}_2\text{O})][\{(\text{Cp}')_2\text{Th}^{\text{III}}\}(\mu^2\text{-H})_3\text{Th}^{\text{IV}}(\text{H})(\text{Cp}')_2]$ , which forms concomitantly with  $(\text{Cp}')_3\text{Th}^{\text{III}}$  (Fig. 19c).<sup>163</sup> Likewise, the rare uranium(II) tris(cyclopentadienyl) complex,  $[\text{K}(2.2.2\text{-cryptand})][\{(\text{Cp}')_3\text{U}^{\text{II}}\}]$ , is readily converted to  $[\text{K}(2.2.2\text{-cryptand})][\{(\text{Cp}')_3\text{U}(\text{H})\}]$  by direct hydrogenation (1 bar, 0 °C),<sup>160</sup> or by treatment with silane.<sup>164</sup>

**Structure, bonding insights & co-ligand effect.** In comparison to that of the lanthanide hydrides, the extent to which actinide hydrides have been characterised is somewhat less complete, hampered by the small number of examples and inconsistency of analyses to which novel materials have been subjected.

**Morphology and connectivity.** At the time of Ephritikhine's 1997 review of the field,<sup>16</sup> very few species yet possessed complete X-ray crystallographic data. Such characterisation of actinide–hydride linkages is necessarily limited by the poor resolution of electron density associated with the hydride

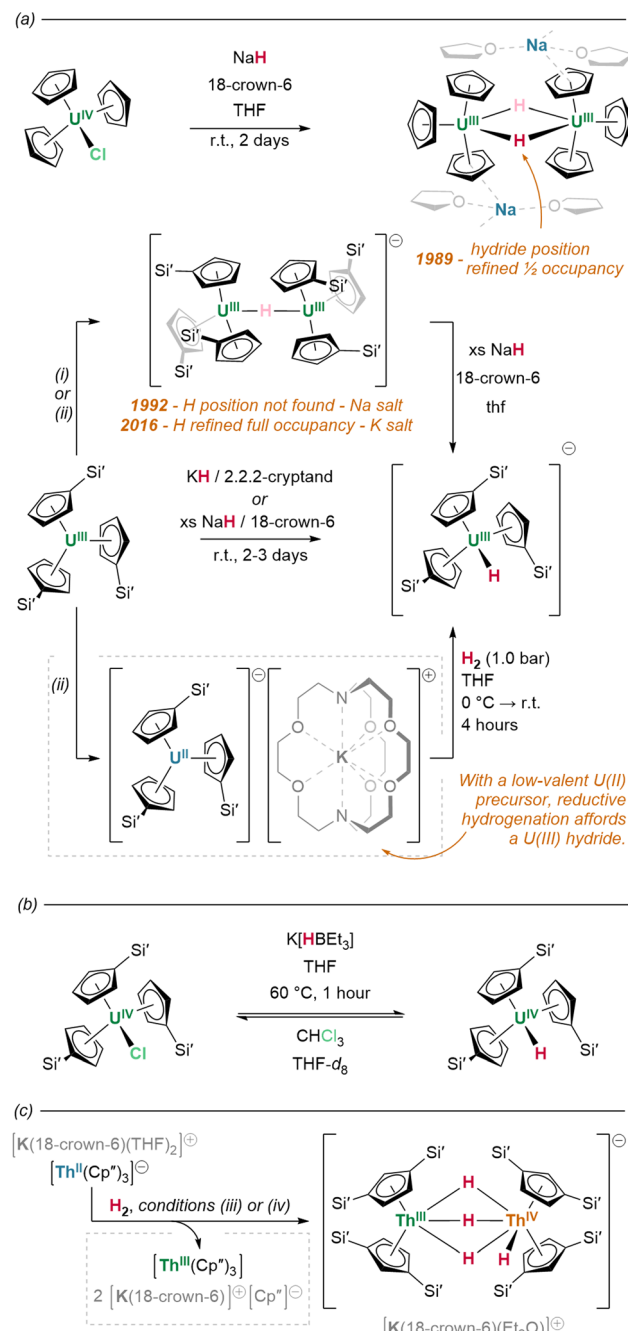


**Fig. 19** Synthesis of hydrides *via* reactions with hydride transfer agents or *via* low-valent actinide species show similarities in their behaviour. (a) In 1989, salt metathesis of  $\text{Cp}_3\text{UCl}$  with  $\text{NaH}$  yielded a mono-hydride bridged dimer which was originally assigned as a crystallographically disordered species with bent hydride bridges exhibiting  $\text{M}-\text{H}-\text{M}$  angles around  $160^{\circ}$ . In 1992, treatment of  $\text{U}^{\text{III}}\text{Cp}'_3$  with  $\text{NaH}$  yielded a dimer with a proposed linear  $\text{M}-\text{H}-\text{M}$  angle; however, no hydride was found. In 2016, Evans *et al.* reported the K analogue and were able to refine the H position in the linear bound site. (i)  $\text{NaH}$ ,  $18\text{-crown-6}$ ,  $\text{thf}$ , 2 days; (ii)  $\text{KC}_8$ ,  $18\text{-crown-6}$ ,  $\text{Et}_2\text{O}$ ,  $-35\text{ }^{\circ}\text{C}$  (iii)  $\text{H}_2$  (4.1 bar), 18 h, solvent free; (iv)  $\text{H}_2$  (1 bar), 20 min,  $\text{thf}$ ,  $0\text{ }^{\circ}\text{C}$  – r.t.



centre, especially in close contact with the substantial electron clouds of uranium or thorium nuclei. Although neutron diffraction methods have enabled a substantially higher level of analysis in a handful of cases, there remains to this day a paucity of this high-quality data.

What solid state structural data does exist suggests a marked change in behaviour compared to the lighter elements of the f-block. In Marks' 1979 report of the first crystallographically-characterised example of a molecular actinide hydride, neutron diffraction identified  $[(\text{Cp}^*)_2\text{Th}(\mu^2\text{-H})(\text{H})]_2$  as a bimetallic tetrahydride complex, wherein the metal centres each possess one terminal hydride ligand, and are bridged between themselves by the two remaining  $\mu^2$  hydrides. The Th-H contacts in the complex differ significantly between coordination modes, with terminal linkages the shorter of the two configurations (terminal: 2.03(1); bridging: 2.29(3) Å).<sup>165</sup> In solution, however, these hydrides exchange readily between modes at room temperature, as evidenced by the indistinguishability of their  $^1\text{H}$  resonances (19.25 ppm) on the NMR timescale.<sup>146</sup> Although this resonance occurs significantly downfield of those associated with typical, diamagnetic late transition metal hydrides, deshielding in complexes of large  $d^0$  ions is known to produce a similar effect.<sup>166</sup>

Similar, dinuclear structures,  $[(\text{L})_2\text{An}(\text{H})]_2$ , occur in a significant proportion of the thorium-containing examples reported to date,<sup>146,147,163,165,167–169</sup> although mononuclear complexes are more common,<sup>152,161,163,169–172</sup> and clusters containing three or more hydride-bridged thorium centres are also represented to varying but lesser degrees.<sup>151,173,174</sup> Amongst uranium examples, dinuclear species predominate,<sup>146,147,149,150,153–155,158,159,168</sup> but a sizeable number of mononuclear complexes are also known.<sup>159,160,172,175–178</sup> Notably, until this year, no higher-order uranium hydride clusters had been reported: Zhu, Maron and colleagues' tetranuclear, *ansa*-bis(cyclopentadienyl)-supported octahydride cluster  $\{(\text{CpCMe}_2\text{CMe}_2\text{Cp})\text{U}^{\text{IV}}\}_4(\mu^2\text{-H})_4(\mu^3\text{-H})_4$  represents only the first such example. Significantly, X-ray diffraction reveals a coplanar arrangement of its uranium centres and conspicuously short U-U distances (3.65–3.70 Å) which approach the sum of single-bond covalent radii for a U-U interaction; the intriguing possibility that this indicates electron delocalisation between the uranium centres themselves is somewhat supported by NBO analyses and the calculation of a U-U Wiberg bond index of 0.39. NBO analyses further characterise U-H bonding modes as delocalised, 3c-2e or 4c-2e bonds which are strongly polarised towards H.<sup>179</sup>

For thorium, complex morphologies depend strongly upon the steric influence of supporting ligand systems—although the differences observed result no less from stoichiometry than the identity of the chosen ligand. With one additional  $\text{Cp}^*$  ligand, the mononuclear, tris(cyclopentadienyl) analogue of  $[(\text{Cp}^*)_2\text{Th}(\text{H})]_2$ ,  $(\text{Cp}^*)_3\text{Th}(\text{H})$ , possesses a single, conspicuously unreactive, terminal hydride; its Th-H contact (2.33(13) Å) compares well with that of its prior congener, although the  $^1\text{H}$  resonance of its singular hydride (15.4 ppm) appears somewhat further upfield.<sup>169</sup> With one fewer ligand per thorium

centre,  $[(\text{Cp}^*)\text{Th}(\text{H})]_7$  exists as a heptanuclear thorium(IV) cluster with all eight hydrides coalescing into a single  $^1\text{H}$  NMR shift at 16.44 ppm.<sup>151</sup>

Uranium examples exhibit marginally less steric strain, differing from those above by oxidation state and cluster order. The direct analogues comprise dinuclear species  $[(\text{Cp}^*)_2\text{U}^{\text{III}}(\mu^2\text{-H})]_2$  and  $[(\text{Cp}^*)_2\text{U}^{\text{IV}}(\text{H})]_2$ ;<sup>147</sup> of further note is the “tuck-in tuck-over” bimetallic complex  $\{(\text{Cp}^*)_2\text{U}\}(\mu^2\text{-H})_2\{\text{U}(\text{Cp}^*)(\text{C}_5\text{Me}_3\{\text{CH}_2\}\{\mu^2\text{-CH}_2\})\}$ , in which two of the methyl substituents of a single pentamethylcyclopentadienyl ligand are metalated and in contact with different uranium centres.<sup>149</sup>

The hydride positions in these latter examples have never been determined crystallographically, and without neutron diffraction data, further structural analysis is only intermittently possible. In a related uranium(III) diphosphine complex,  $(\text{Cp}^*)_2\text{U}^{\text{III}}(\text{H})(\text{dmpe})$  ( $\text{dmpe} = 1,2\text{-}(\text{dimethylphosphino})\text{ethane}$ ), its hydride position was deduced from geometric considerations;<sup>177</sup> a reported thorium(IV) congener,  $[(\text{Cp}^*)_4\text{Th}^{\text{IV}}]_2(\text{dmpe})\text{BPh}_4$ , is proposed to adopt a bimetallic configuration but has not been crystallographically characterised.<sup>169</sup> Despite the crystallographic identification of  $(\text{N}^*)\text{U}^{\text{IV}}(\text{H})$ , the position of its hydride ligand could not be refined; its presence can only be inferred from the tetravalent oxidation state of the metal.<sup>172</sup>

Considered modifications made to the steric profiles of ligands may represent a route to more subtly influence complex structures (Fig. 20). With only the absence of one ligand methyl substituent, mononuclear  $(\text{Cp}^*)_3\text{Th}^{\text{IV}}(\text{H})$  remains a close comparator of  $(\text{Cp}^*)_3\text{Th}^{\text{IV}}(\text{H})$ ;<sup>163</sup> in the monoligated mode, however, the corresponding cluster is octanuclear  $[(\text{Cp}^*)\text{Th}^{\text{IV}}(\mu^2\text{-H})]_8$ . Conversely, exchanging a methyl for a trimethylsilyl substituent affords hexanuclear  $[(\text{Cp}^*)\text{Th}^{\text{IV}}(\mu^2\text{-H})]_6$ . Stepping beyond minor alterations, two even more sterically substantial congeners,  $[(\text{Cp}^{\text{R}})\text{Th}^{\text{IV}}(\mu^2\text{-H})]_5$  ( $\text{Cp}^{\text{R}} = \text{Cp}^{\text{tt}}, \text{Cp}''; \text{Cp}^{\text{tt}} = 1,2,4\text{-}(\text{Bu})_3\text{C}_5\text{H}_2; \text{Cp}'' = 1,2,4\text{-}(\text{SiMe}_3)_3\text{C}_5\text{H}_2$ ), crystallise instead as a pentamer. These thorium clusters differ from comparable lanthanide examples in that only  $\mu^2$ - and  $\mu^3$ -bridging hydrides have yet been identified in crystallographically-authenticated structures; however, it remains the case that average hydride coordination number increases with cluster order. Between thorium examples, morphologies differ dramatically: while  $[(\text{Cp}^*)\text{Th}(\text{H})]_8$  adopts a distorted square-antiprismatic arrangement of its eight thorium centres,  $[(\text{Cp}^*)\text{Th}^{\text{IV}}(\text{H})]_7$  is a distorted pentagonal bipyramidal,  $[(\text{Cp}^{\text{R}})\text{Th}^{\text{IV}}(\text{H})]_6$  approximates an octahedron, and  $[(\text{Cp}^{\text{tt}})\text{Th}^{\text{IV}}(\mu^2\text{-H})]_5$  a square-based pyramid. In  $[(\text{Cp}^{\text{R}})]_{12}\text{Th}_{13}\text{H}_{40}$ , although hydride positions could not be refined, a tetrahedron of  $\{(\text{Cp}^{\text{R}})\text{Th}\}_3$  units encapsulates a single thorium centre.<sup>151</sup>

**Spectroscopic insights.** Whilst a number of uranium hydrides have been characterised by NMR spectroscopy, the paramagnetic nature of uranium oxidation states III–V precludes any useful discussion thereof.<sup>180</sup> In principle, the diamagnetism of thorium(IV) complexes enables more considered commentary, although hydride shifts are more indicative of ligand electronics than cluster size. For example, whilst the hydrides of  $[(\text{Cp}^{\text{tt}})\text{Th}^{\text{IV}}(\mu^2\text{-H})]_5$  give rise to a resonance at

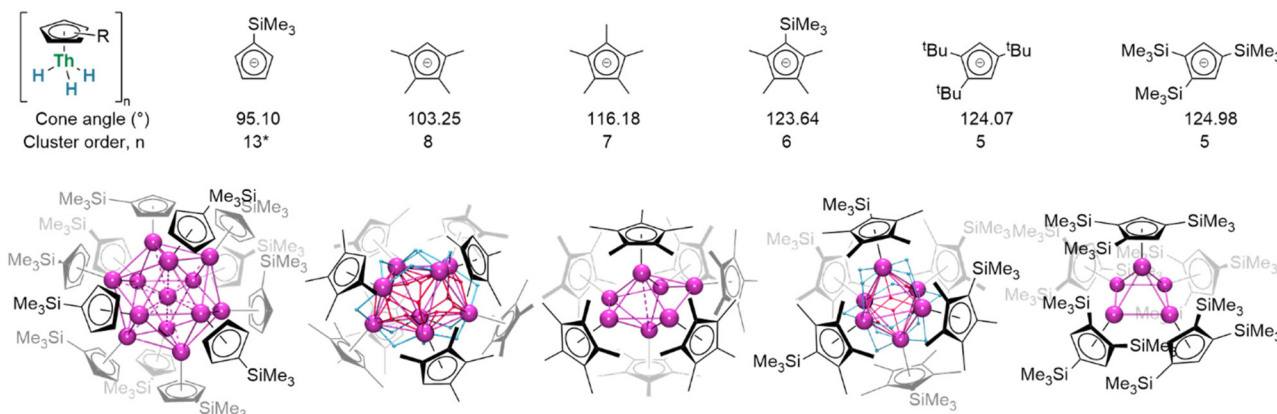


**Fig. 20** Cluster order decreases with increasing with cyclopentadienyl ligand cone angle, measured from solid state structures. \* The  $\text{Cp}'$  ligand results in a complex cluster of the form  $\{(\text{Cp}'\text{Th})_3(\text{H})_{10}\}_4\text{Th}$  in which the position of the hydrides is unknown. Despite its non-standard nature it is clear than this ligand can, and does, facilitate for formation of higher-order clusters than its smaller analogues. This cluster is also reminiscent of the structure of binary hydride  $\text{Th}_4\text{H}_{15}$ .

16.46 ppm in  $\text{C}_6\text{D}_6$ , the replacement of *tert*-butyl substituents with more electropositive trimethylsilyl groups in  $[(\text{Cp}'')\text{Th}^{\text{IV}}(\mu^2\text{-H})_3]_5$  leads its analogous resonance to appear somewhat further upfield, at 15.78 ppm. A much more subtle effect is observed when ligand sterics, rather than electronics, are modulated: the hydrides of heptameric  $[(\text{Cp}^*)\text{Th}(\mu^2\text{-H})_3]_7$  and octameric  $[(\text{Cp}^*)\text{Th}(\mu^2\text{-H})_3]_8$  give rise to resonances at 16.68 ppm and 16.44 ppm—virtually indistinguishable from those of  $[(\text{Cp}^{\text{ttt}})\text{Th}(\mu^2\text{-H})_3]_5$ .

IR spectroscopy can provide complementary insights where other techniques are limited. In general,  $\text{An}-\text{H}$  vibrations appear at slightly higher frequencies ( $1200$  to  $1500\text{ cm}^{-1}$ ) than those of their lanthanide congeners, and there are also discernible differences in vibrational energies between the hydrides of isostructural thorium and uranium complexes, such as  $(\text{N}^{\text{v}})_3\text{An}(\text{H})$  ( $\text{An} = \text{Th}$ ,  $\nu_{\text{Th}-\text{H}} = 1480\text{ cm}^{-1}$ ;  $\text{An} = \text{U}$ ,  $\nu_{\text{U}-\text{H}} = 1430\text{ cm}^{-1}$ ). This discernibility is also retained upon deuteration, whereupon bands are instead observed at  $1060$  and  $1020\text{ cm}^{-1}$  respectively.<sup>181,182</sup> Unfortunately, the availability and assignment of IR spectral data in the literature has been somewhat limited to date; its inclusion in future publications is likely to offer new insights.

**Redox behaviour and reactivity towards substrates.** Among the greatest opportunities for future research, however, may yet be found in the reactivity of actinide hydrides. In some respects, this conforms to trends established elsewhere in the periodic table: the characteristic reactivity of hydride species towards haloalkanes makes treatment with  $\text{CCl}_4$  a common chemical test for transition metal hydrides; this is also found to be effective in a number of actinide cases.<sup>163,175,179</sup> Actinide hydrides may also participate in some of the same catalytic hydroelementation processes as lanthanides.<sup>183,184</sup> Additionally, bimetallic  $[(\text{Cp}^*)_2\text{Th}(\mu^2\text{-H})_2]_2$  is conventionally reducible in the presence of  $\text{KC}_8$  and 18-crown-6, although the resulting trivalent complex is challenging to isolate.<sup>163</sup>

In other respects, their chemistry can differ dramatically. Whilst the potentiality of these f-block species has not yet

been fully-established by comprehensive studies, in individual cases, detailed investigations have begun to illustrate the divergence and potential utility of their reactivity. A case worth considering in this context is that of Meyer and colleagues' trivalent scaffold complex,  $\{(\text{Ad},\text{MeArO})_3\text{mes}\}\text{U}^{\text{III}}$ , which undergoes an isomerization process upon reduction with  $\text{KC}_8$  or  $\text{Na}^0$  wherein  $\text{H}^{\cdot}$ , abstracted from the benzylic methylene linker of one arm of the supporting ligand, migrates to the metal centre (Fig. 8d); here, it bridges between the uranium centre and an alkali metal centre, which is itself  $\eta^4$ -coordinated to the most proximate aryloxide moiety of the ligand. However, abstraction of the respective alkali metal centres by treatment with an appropriate encapsulation agent (18-crown-6, 15-crown-5) also induces the insertion of hydride into the central arene ring, disrupting its aromaticity.<sup>175</sup> Such an actinide-mediated rearrangement is at least suggestive of a novel dearomatisation strategy. Of course, as is true in this case, not all such reactivity is welcome; the aforementioned decomposition of suitably-ligated hydride species, eliminating  $\text{H}_2$  to yield cyclometalated 'tuck-in' complexes, is indicative of the precarious balance of factors which keep these complexes stable. When reactions are reversible—as in the case of  $(\text{COT}^{\text{TPS}^2})(\text{Cp}^*)\text{U}(\text{H})$ , which exists in an equilibrium balanced by its 'tuck-in' analogue and  $\text{H}_2$ —this can somewhat complicate the interpretation of complex reactivity.<sup>176</sup>

Of some further interest is the potential for hydrides to exhibit redox activity, even in the absence of a typically redox-active metal (e.g. thorium, for which the tetravalent oxidation state overwhelmingly predominates):  $[(\text{Cp}^*)_2\text{Th}^{\text{IV}}(\mu^2\text{-H})(\text{H})]_2$ , generated *in situ*, reacts with  $\text{S}_8$  to form  $(\text{Cp}^*)_2\text{Th}^{\text{IV}}(\text{S}_5)$  (Fig. 21); its uranium(IV) analogue reacts with 2,2'-bipyridine to yield  $(\text{Cp}^*)_2\text{U}^{\text{IV}}(\text{bipy})$ , wherein the reduction of the 2,2'-bipyridyl ligand is achieved without any ultimate change in the metal oxidation state.<sup>162</sup>

Alternatively, reactions of actinide hydrides with small molecules demonstrate the surprising potential for actinide hydride-mediated functionalization of organic fragments.

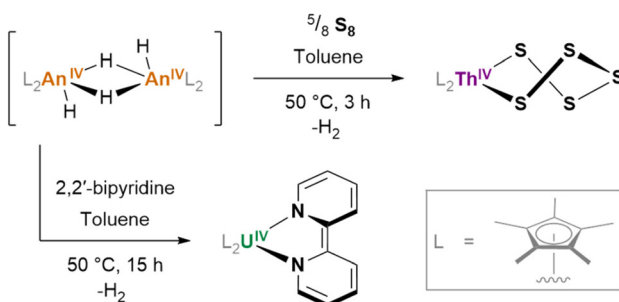


**Fig. 21** Actinide hydride reduction behaviour towards substrates.  $[\text{Cp}^*\text{Th}]_2(\text{H})_4$  generated *in situ* reacts with elemental sulfur to yield form a  $\text{S}_5^{2-}$  coordinated product. The analogous uranium hydride,  $[\text{Cp}^*\text{U}]_2(\text{H})_4$ , reacts with 2,2'-bipyridine to coordinate the reduced bipyridyl dianion ( $\text{bipy}^{2-}$ ).

Treatment of  $[(\text{Cp}^*)_2\text{U}(\mu^2\text{-H})]_2$  with MeCN (6 equiv.) induces the condensation of three MeCN units to  $(\text{C}_6\text{N}_3\text{H}_7)^{2-}$ , which binds in a  $\kappa^2\text{-N},\text{N}'$  fashion, bridging the two uranium(IV) centres (Fig. 22, top left). Of further significance is that dithorium(IV) tetrahydride complex  $[(\text{Cp}^*)_2\text{Th}(\mu^2\text{-H})(\text{H})]_2$  may be considered to possess similar reactivity to U(III) containing  $[(\text{Cp}^*)_2\text{U}(\text{H})]_2$ . It, likewise, undergoes reaction with MeCN to generate  $(\text{C}_6\text{N}_3\text{H}_7)^{2-}$  (Fig. 22, top right).<sup>168</sup> Previously-mentioned  $\text{Cs}[\{(\text{Si}^{\text{O}^+}\text{O})_3\text{U}\}_2(\mu^2\text{-H})(\mu^2\text{-NH})]$  also undergoes reaction with MeCN to give  $\text{Cs}[\{(\text{Si}^{\text{O}^+}\text{O})_3\text{U}\}_2(\mu^3\text{-NH})(\mu^2\text{-NCHCH}_3)]$

(Fig. 22, middle), in which the  $\mu^3$ -imido ligand also coordinates  $\text{Cs}^+$ . In the presence of  $\text{CO}_2$  (2 equiv.), insertion into both the U-H and U-NH linkages of  $\text{Cs}[\{(\text{Si}^{\text{O}^+}\text{O})_3\text{U}\}_2(\mu^2\text{-H})(\mu^2\text{-NH})]$  yields  $\text{Cs}[\{(\text{Si}^{\text{O}^+}\text{O})_3\text{U}\}_2(\mu^2\text{-HCOO})(\mu^2\text{-NHCOO})]$ .<sup>153</sup> In a further expansion on this concept, sequential reactions of related  $\text{K}_2[\{(\text{Si}^{\text{O}^+}\text{O})_3\text{U}\}_2(\mu^2\text{-O})(\mu^2\text{-H})_2]$  with a range of small molecules demonstrate the efficacy of transfer hydrogenation at actinide centres, enabling the assembly of entire organic fragments (Fig. 22, bottom). By a two-electron process, the complex reductively couples MeCN to form  $(\text{NC}(\text{CH}_3)\text{NCH}_2\text{CH}_2)^{2-}$ , a dianionic fragment which may be isolated in a  $\mu^2\text{:}\kappa^2$  bridging mode between its two uranium centres alongside its pre-existing  $\mu^2$ -oxo. Alternatively, treatment with CO results in the formation of an  $(\text{OCH}_2)^{2-}$  fragment, whereafter further treatment with  $\text{H}_2$  (1 bar, r.t.) affords  $(\text{OCH}_3)^-$  and reintroduces a hydride ligand. From either the  $(\text{OCH}_2)^{2-}$  bridged complex, or after further reaction of the  $(\text{OCH}_3)^-$  bridged complex with  $\text{CO}_2$ , separable organic compounds  $\text{CH}_2\text{DOD}$ —or, in the latter case, a mixture of formate, bicarbonate, and methanol—may be identified by NMR spectroscopy after treatment of the complex with  $\text{D}_2\text{O}$ .<sup>150</sup>

**Related insights: a dihydrogen complex.** As a final note: albeit not a study of conventional hydride complexes, significant insights into the nature of actinide–hydrogen linkages may also be gleaned from related dihydrogen complexes. Only very recently has the first evidence for the formation of such an actinide complex been reported: by utilising the pseudocon-

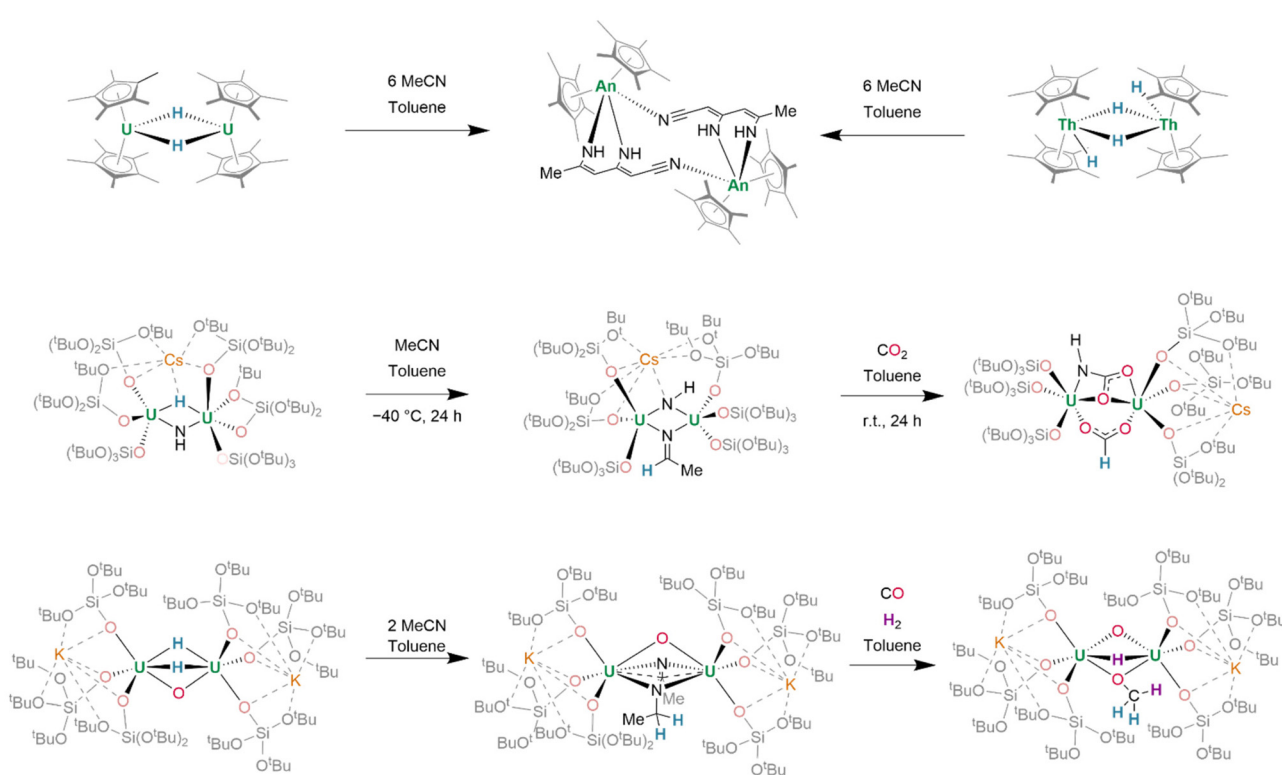


**Fig. 22** Reactivity of actinide hydrides towards unsaturated small molecules. (a) Actinide metallocene hydrides facilitate  $\beta$ -coupling of nitriles. (b) and (c) U(IV) mono and dihydrides can facilitate hydride transfer to nitriles with C–N coupling in the latter case. In both cases further transfer of the hydrides to other unsaturated small molecules is possible.



tact shift in  $^1\text{H}$  NMR spectroscopy, Bergman and Arnold were able to observe the formation of  $(\text{Cp}')_3\text{U}^{\text{III}}(\eta^2\text{-H}_2)$  by titration of  $\text{H}_2$  into benzene- $d_6$  solutions of unsolvated  $(\text{Cp}')_3\text{U}^{\text{III}}$ . Supporting computational analysis by Maron indicates that no  $\sigma$ -bonding U-H interactions, nor any polarisation of the H-H bond, are present in this compound—the metal instead donates from a 5f orbital to generate a  $\pi$ -bonding interaction, concomitantly elongating the H-H bond—and, furthermore, the U...( $\text{H}_2$ ) interaction in the geometry-optimised structure is significantly shorter than in its only identified lanthanide comparator,  $(\text{Cp}^*)_2\text{Eu}^{\text{II}}(\text{H}_2)$ . It is curious, then, that the  $^1\text{H}$  NMR pseudocontact shifts induced by both complexes are similar in magnitude, when this should be expected to be much greater in the uranium(III) case; this is rationalised as the result of a less favourable U...( $\text{H}_2$ ) interaction as compared to the europium(II) example.<sup>185</sup> These observations reinforce evidence that, although typically small in magnitude, covalent contributions to bonding in uranium-ligand interactions (in this instance, a rare case of back-donation from the actinide centre) produce discernible physical differences compared to other f-block complexes.

### Bridging and Lewis acid coordinated actinide hydrides

**Actinide borohydrides.** Although actinide borohydride complexes constitute a substantial subfield in their own right, the majority of examples utilise borohydride solely as a readily replaceable pseudohalide ligand.<sup>186–188</sup> Representatively, trivalent borohydrides such as  $[\text{U}^{\text{III}}(\text{BH}_4)_3(\text{thf})_2]$  have shown utility as starting materials for the preparations of several novel uranium complexes of highly reducing arene ligands. These species are challenging to prepare from more conventional halide starting materials, from which reactions are instead reported to generate metallic uranium and uncharacterisable organic products.<sup>189–192</sup>

Such divergent reactivity suggests a structural cause. Coordination of group XIII metal hydrides to actinide centres characteristically involves  $\text{An}\cdots\text{H}-\text{M}$  bridging interactions, wherein the hydrides span the metal centres in a 3c-2e bonding configuration. Sharing either two or three hydrides between actinide and group XIII metal centres, both  $\mu^2$ - and  $\mu^3$ -bridging modes are observed crystallographically in the iso-morphous, homoleptic, tetravalent borohydrides,  $[\text{U}(\text{BH}_4)_4]$  and  $[\text{Th}(\text{BH}_4)_4]$ .<sup>193,194</sup> That there is a degree of covalency in these linkages is supported by their volatility:  $[\text{U}(\text{BH}_4)_4]$  sublimes at temperatures as low as 30 °C, and the volatility of its transuranic analogues is reportedly even greater; these materials exist as pyrophoric liquids which decompose readily at room temperature.<sup>195,196</sup> Conspicuously, sublimation of its thorium congener requires temperatures at least 100 degrees higher.<sup>196</sup> Furthermore, in an intriguingly straightforward procedure, it has been demonstrated by Daly and colleagues that  $\text{U}(\text{BH}_4)_4$  is reducible to uranium(III) merely by heating the tetravalent borohydride to 100 °C under argon, offering facile access to this low oxidation state.<sup>197</sup>

Evidently, the capacity for variable bridging modes is important: alongside their relative lability, these factors likely

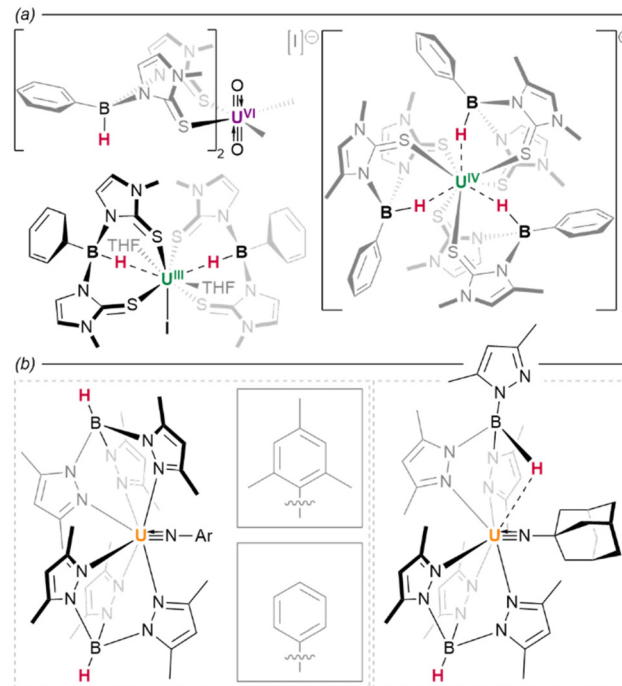


**Fig. 23** Borohydride complexes of actinides. (a) With bis(pyrazolyl) borane and bis(methimazolyl)boranes coordination of the B-H bond to the actinide centre is facile. (b) With tris(pyrazolyl)boranes the flexibility in coordination mode may allow for formation of complexes with more sterically encumbered co-ligands.

offer complexes a degree of flexibility in their coordination spheres which cannot be achieved using comparable halides. The magnitude of U...H interactions have been quantified spectroscopically in hydrobis(mercaptoimidazolyl)borate (tim<sup>Me</sup>) complex  $\text{U}\{\text{B}(\text{H})(\text{R})(\text{tim}^{\text{Me}})_2\}_2(\text{thf})_2$  ( $\text{R} = \text{H, Ph}$ ), wherein a trivalent uranium centre is stabilised by tridentate ligands capable of enforcing a single U...H-B interaction per ligand (Fig. 23a). Straightforward IR spectroscopic observation of a shift in B-H stretching frequencies between the free (2446  $\text{cm}^{-1}$ ) and coordinated (2376  $\text{cm}^{-1}$ ) ligand is suggestive of a  $\kappa^3\text{-H,S,S}$ -binding mode—although U-H distances are significantly elongated ( $\text{R} = \text{H, 2.31(9) \AA}$ ;  $\text{R} = \text{Ph, 2.54(9) \AA}$ ) relative to direct actinide hydrides.<sup>198</sup> In a further illustrative case, Bart and colleagues have observed a sterically-induced change in the coordination mode of a tris(pyrazolyl)borate ligand, which occurs upon introduction of imide ligands bearing substituents of differing steric size. Whereas the supporting ligands of  $(\text{Tp}^*)_2\text{U}^{\text{IV}}(\text{NR})$  ( $\text{R} = \text{mes, Ph}$ ) both adopt typical  $\kappa^3\text{-N, N,N}$  coordination modes to the uranium(IV) centre, the more substantial adamanyl substituent in  $(\text{Tp}^*)_2\text{U}^{\text{IV}}(\text{NAd})$  enforces a change to an unsymmetrical configuration, wherein one ligand instead binds in a  $\kappa^3\text{-N,N,H}$  fashion with one of the pyrazolyl arms of the ligand in the apical position Fig. 23b.<sup>199</sup>

**Heterobimetallic hydrides.** Tetravalent, heterobimetallic alanate-hydride complex  $(\text{Cp}^*)_2\text{Th}^{\text{IV}}(\text{H})\{\mu^2\text{-H}_3\text{Al}(\text{Si}')_3\}$ , alongside its trivalent alanate congener,  $(\text{Cp}^*)_2\text{Th}^{\text{III}}\{\mu^2\text{-H}_3\text{Al}(\text{Si}')_3\}$ , exhibit modest structural differences between themselves—as



well as compared to their uranium(III) analogue,  $(\text{Cp}^\dagger)_2\text{U}\{\text{H}_3\text{Al}(\text{Si}^\dagger)_3\}$ . Of key interest in the latter two examples is the possibility, supported by DFT calculations, that  $\text{An}^{\text{III}}\cdots\text{H-Al}$  interactions stabilise the first reported example of a dative  $\text{An} \rightarrow \text{M}$  interaction (Fig. 15b). Curiously, there is describedly a greater degree of  $\text{An} \rightarrow \text{Al}$  charge transfer character in the thorium(III) case than for either its uranium(III) or titanium(III) analogues.<sup>200</sup>

There are few examples of heterobimetallic actinide complexes incorporating transition metal hydrides; however, recent work by the Arnold and Camp groups has also characterised hydride-supported  $\text{An} \rightarrow \text{M}$  interactions with iridium. The isolated complexes,  $\{(\text{Cp}^*)\text{Ir}(\text{H})_3\}_4\text{U}^{\text{IV}}$  and  $\{(\text{Cp}^*)\text{Ir}(\text{H})_3\}_4\text{Th}^{\text{IV}}$ , wherein the respective actinide centres are twelve- and ten-coordinate, are calculated to possess notably high Wiberg  $\text{An}-\text{M}$  bond indices ( $\text{U} \rightarrow \text{Ir} = 0.97$ ;  $\text{Th} \rightarrow \text{Ir} = 0.65$ ).<sup>201</sup>

## Conclusions

In this perspective, we have illustrated the key synthetic pathways for the synthesis of lanthanide and actinide hydrides, with hydrogenolysis and  $\sigma$ -bond metathesis reactions from metal alkyls being the most widely utilised. Our analysis suggests that sequential hydrogenolysis of metal alkyls is slower as the number of alkyl groups increases on a metal due to the formation of highly bridged hydride intermediates. In addition, hydrogenolysis appears to be facilitated greatly by metalated ligand intermediates which contain ring-strained metallacycles. Only a few examples of hydrides formed from, or with, low-oxidation state f-block metals are known; however, what has been reported to date suggests a key role for reduced arene ligands in their formation by this pathway.

In terms of structure, the order of clusters is shown to grow as co-ligand stoichiometry and sterics decrease, in order to retain high coordination numbers on the metals. The structure of these clusters also changes with metal ion size with smaller lanthanides, in particular, able to invoke  $\mu^4$  and even  $\mu^6$  coordination modes for the hydride, mirroring the ionic bonding in binary hydrides. At the opposite end of the covalency spectrum, evidence has now been presented for the formation of both lanthanide and actinide dihydrogen complexes, though current evidence suggests bonding is very different between the two periods.

The reactivity of lanthanide hydrides comprises primarily  $\sigma$ -bond metathesis and 1,2-addition reactions due to their limited access to redox reactivity; however, these two powerful mechanisms have been exploited to great effect in catalytic polymerisation, hydrogenation and hydroelementation.

In this work, we have outlined how cluster structure and nuclearity can influence reactivity, with highly bridged hydrides reacting more slowly with some substrates. This should inform choice of co-ligand for lanthanide pre-catalysts which invoke hydrides in the catalytic cycle. For actinides, different pathways may operate, allowing for coupling of nitrile ligands for example, rather than simple 1,2-addition; transfer

hydrogenation of small molecules; and redox-like reactivity for thorium(IV) hydrides.

Bridging hydrides are also shown to stabilise a wide range of complexes of the form  $\text{Ln}\cdots\text{H-E/Ln}\cdots\text{H-M}$  with varying  $\text{Ln-E/Ln-M}$  interactions from the extreme of  $\text{Ln-E}$  bonds with agostic interactions to  $\text{An} \rightarrow \text{M}$  species where a low-valent actinide is able to act as a Lewis base toward an electron-deficient metal centre.

Together, this survey presents an emerging picture of the field of f-block hydrides which is beginning to understand how to employ fine electronic and structural control to exploit the distinctive characteristics of complexes which span the full length and breadth of the periodic table.

## Author contributions

This manuscript was conceived by Dr Bell and written together by both Dr Bell and Dr Drummond Turnbull, including preparation of all figures.

## Conflicts of interest

There are no conflicts to declare.

## Acknowledgements

The authors would like to acknowledge the EPSRC (Open Fellowship EP/W02702X/1) and the University of Glasgow (LKAS Fellowship) for funding this work.

## Notes and references

- 1 J. Hutchinson, J. Alwin, A. McSpaden, W. Myers, M. Rising and R. Sanchez, *Nucl. Technol.*, 2021, **207**, S62–S80.
- 2 H. Liu and M. S. Eisen, *Synthesis*, 2020, **52**, 629–644.
- 3 W. Chen, J. Li and C. Cui, *Synlett*, 2020, **32**, 962–970.
- 4 H. Sugiyama, T. Nakao, M. Miyazaki, H. Abe, Y. Niwa, M. Kitano and H. Hosono, *ACS Catal.*, 2022, **12**, 12572–12581.
- 5 H. Yan, W. Gao, J. Cui, W. Zhang, Q. Pei, Q. Wang, Y. Guan, S. Feng, H. Wu, H. Cao, J. Guo and P. Chen, *J. Energy Chem.*, 2022, **72**, 1–7.
- 6 A. Habibzadeh, M. A. Kucuker and M. Gökelma, *ACS Omega*, 2023, **8**, 17431–17445.
- 7 F. Nafezarefi, H. Schreuders, B. Dam and S. Cornelius, *Appl. Phys. Lett.*, 2017, **111**, 103903.
- 8 J. M. Haschke and T. H. Allen, *J. Alloys Compd.*, 2001, **320**, 58–71.
- 9 A. Banos, N. J. Harker and T. B. Scott, *Corros. Sci.*, 2018, **136**, 129–147.
- 10 A. Banos and T. B. Scott, *Sci. Rep.*, 2020, **10**, 9479.
- 11 F. Peng, Y. Sun, C. J. Pickard, R. J. Needs, Q. Wu and Y. Ma, *Phys. Rev. Lett.*, 2017, **119**, 107001.



12 Z. M. Geballe, H. Liu, A. K. Mishra, M. Ahart, M. Somayazulu, Y. Meng, M. Baldini and R. J. Hemley, *Angew. Chem., Int. Ed.*, 2018, **57**, 688–692.

13 D. V. Semenok, A. G. Kvashnin, A. G. Ivanova, V. Svitlyk, V. Y. Fominski, A. V. Sadakov, O. A. Sobolevskiy, V. M. Pudalov, I. A. Troyan and A. R. Oganov, *Mater. Today*, 2020, **33**, 36–44.

14 M. Falcone, L. Chatelain, R. Scopelliti, I. Živković and M. Mazzanti, *Nature*, 2017, **547**, 332–335.

15 L. Perrin, L. Maron and O. Eisenstein, *Faraday Discuss.*, 2003, **124**, 25–39.

16 M. Ephritikhine, *Chem. Rev.*, 1997, **97**, 2193–2242.

17 P. Vajda, *Solid State Ionics*, 2004, **168**, 271–279.

18 H. Mizoguchi, M. Okunaka, M. Kitano, S. Matsuishi, T. Yokoyama and H. Hosono, *Inorg. Chem.*, 2016, **55**, 8833–8838.

19 R. Griessen, J. N. Huiberts, M. Kremers, A. T. M. van Gogh, N. J. Koeman, J. P. Dekker and P. H. L. Notten, *J. Alloys Compd.*, 1997, **253–254**, 44–50.

20 F. J. A. den Broeder, S. J. van der Molen, M. Kremers, J. N. Huiberts, D. G. Nagengast, A. T. M. van Gogh, W. H. Huisman, N. J. Koeman, B. Dam, J. H. Rector, S. Plota, M. Haaksma, R. M. N. Hanzen, R. M. Jungblut, P. A. Duine and R. Griessen, *Nature*, 1998, **394**, 656–658.

21 W. Zhang, J. Cui, S. Wang, H. Cao, A. Wu, Y. Xia, Q. Jiang, J. Guo, T. He and P. Chen, *Nature*, 2023, **616**, 73–76.

22 S. P. Willson and L. Andrews, *J. Phys. Chem. A*, 2000, **104**, 1640–1647.

23 X. Wang, L. Andrews, I. Infante and L. Gagliardi, *J. Phys. Chem. A*, 2009, **113**, 12566–12572.

24 I. Infante, L. Gagliardi, X. Wang and L. Andrews, *J. Phys. Chem. A*, 2009, **113**, 2446–2455.

25 O. T. Summerscales, E. R. Batista, B. L. Scott, M. P. Wilkerson and A. D. Sutton, *Eur. J. Inorg. Chem.*, 2016, 4551.

26 W. Fegler, A. Venugopal, T. P. Spaniol, L. Maron and J. Okuda, *Angew. Chem., Int. Ed.*, 2013, **52**, 7976.

27 S.-S. Liu, S. Gao, J. W. Ziller and W. J. Evans, *Dalton Trans.*, 2014, **43**, 15526.

28 M. E. Fieser, T. J. Mueller, J. E. Bates, J. W. Ziller, F. Furche and W. J. Evans, *Organometallics*, 2014, **33**, 3882.

29 L. Maron, E. L. Werkema, L. Perrin, O. Eisenstein and R. A. Andersen, *J. Am. Chem. Soc.*, 2005, **127**, 279.

30 H. Kulinna, T. P. Spaniol and J. Okuda, *J. Organomet. Chem.*, 2013, **744**, 49.

31 A. Venugopal, F. Tuna, T. P. Spaniol, L. Ungur, L. F. Chibotaru, J. Okuda and R. A. Layfield, *Chem. Commun.*, 2013, **49**, 901.

32 A. Venugopal, W. Fegler, T. P. Spaniol, L. Maron and J. Okuda, *J. Am. Chem. Soc.*, 2011, **133**, 17574.

33 M. T. Dumas, G. P. Chen, J. Y. Hu, M. A. Nascimento, J. M. Rawson, J. W. Ziller, F. Furche and W. J. Evans, *J. Organomet. Chem.*, 2017, **849–850**, 38.

34 E. Abinet, D. Martin, S. Standfuss, H. Kulinna, T. P. Spaniol and J. Okuda, *Chem. – Eur. J.*, 2011, **17**, 15014.

35 S. Arndt, P. Voth, T. P. Spaniol and J. Okuda, *Organometallics*, 2000, **19**, 4690.

36 K. R. D. Johnson, B. L. Kamenz and P. G. Hayes, *Organometallics*, 2014, **33**, 3005.

37 Y. Takenaka and Z. Hou, *Organometallics*, 2009, **28**, 5196.

38 M. Nishiura, J. Baldamus, T. Shima, K. Mori and Z. Hou, *Chem. – Eur. J.*, 2011, **17**, 5033.

39 G. Desurmont, Y. Li, H. Yasuda, T. Maruo, N. Kanehisa and Y. Kai, *Organometallics*, 2000, **19**, 1811.

40 P. W. Roesky, U. Denninger, C. L. Stern and T. J. Marks, *Organometallics*, 1997, **16**, 4486.

41 X. Shi, P. Deng, T. Rajeshkumar, L. Zhao, L. Maron and J. Cheng, *Chem. Commun.*, 2021, **57**, 10047.

42 J. Cheng, T. Shima and Z. Hou, *Angew. Chem., Int. Ed.*, 2011, **50**, 1857.

43 J. Cheng, M. J. Ferguson and J. Takats, *J. Am. Chem. Soc.*, 2010, **132**, 2.

44 J. Cheng, K. Saliu, M. J. Ferguson, R. McDonald and J. Takats, *J. Organomet. Chem.*, 2010, **695**, 2696.

45 G. M. Ferrence, R. McDonald and J. Takats, *Angew. Chem., Int. Ed.*, 1999, **38**, 2233.

46 Y. Wang, I. D. Rosal, G. Qin, L. Zhao, L. Maron, X. Shi and J. Cheng, *Chem. Commun.*, 2021, **57**, 7766.

47 J. Cheng and Z. Hou, *Chem. Commun.*, 2012, **48**, 814.

48 T. Li, M. Nishiura, J. Cheng, W. Zhang, Y. Li and Z. Hou, *Organometallics*, 2013, **32**, 4142.

49 M. Konkol, T. P. Spaniol, M. Kondracka and J. Okuda, *Dalton Trans.*, 2007, 4095.

50 W. Chen, H. Song, J. Li and C. Cui, *Angew. Chem., Int. Ed.*, 2020, **59**, 2365.

51 J. Liu, W. Chen, J. Li and C. Cui, *ACS Catal.*, 2018, **8**, 2230.

52 T. Dube, S. Gambarotta and G. P. A. Yap, *Organometallics*, 2000, **19**, 817.

53 T. Dube, S. Gambarotta and G. Yap, *Organometallics*, 2000, **19**, 121.

54 C. Wang, L. Xiang, X. Leng and Y. Chen, *Dalton Trans.*, 2017, **46**, 1218.

55 Q. Wen, B. Feng, L. Xiang, X. Leng and Y. Chen, *Inorg. Chem.*, 2021, **60**, 13913.

56 O. Tardif, M. Nishiura and Z. Hou, *Tetrahedron*, 2003, **59**, 10525.

57 D. Cui, M. Nishiura, O. Tardif and Z. Hou, *Organometallics*, 2008, **27**, 2428.

58 O. Tardif, M. Nishiura and Z. Hou, *Organometallics*, 2003, **22**, 1171.

59 D. M. Lyubov, A. M. Bubnov, G. K. Fukin, F. M. Dolgushin, M. Yu. Antipin, O. Pelce, M. Schappacher, S. M. Guillaume and A. A. Trifonov, *Eur. J. Inorg. Chem.*, 2008, 2090.

60 W. Rong, D. He, M. Wang, Z. Mou, J. Cheng, C. Yao, S. Li, A. A. Trifonov, D. M. Lyubov and D. Cui, *Chem. Commun.*, 2015, **51**, 5063.

61 A. A. Trifonov, E. A. Fedorova, G. K. Fukin and M. N. Bochkarev, *Eur. J. Inorg. Chem.*, 2004, 4396.

62 A. A. Trifonov, G. G. Skvortsov, D. M. Lyubov, N. A. Skorodumova, G. K. Fukin, E. V. Baranov and V. N. Glushakova, *Chem. – Eur. J.*, 2006, **12**, 5320.



63 G. M. Richardson, I. Douair, S. A. Cameron, J. Bracegirdle, R. A. Keyzers, M. S. Hill, L. Maron and M. D. Anker, *Nat. Commun.*, 2021, **12**, 3147.

64 C. Ruspic, J. Spielmann and S. Harder, *Inorg. Chem.*, 2007, **46**, 5320.

65 Z. Hou, Y. Zhang, O. Tardif and Y. Wakatsuki, *J. Am. Chem. Soc.*, 2001, **123**, 9216.

66 D. M. Lyubov, A. V. Cherkasov, G. K. Fukin, S. Yu. Ketkov, A. S. Shavyrin and A. A. Trifonov, *Dalton Trans.*, 2014, **43**, 14450.

67 D. M. Lyubov, C. Doring, S. Yu. Ketkov, R. Kempe and A. A. Trifonov, *Chem. – Eur. J.*, 2011, **17**, 3824.

68 N. S. Radu and T. D. Tilley, *J. Am. Chem. Soc.*, 1995, **117**, 5863–5864.

69 I. Castillo and T. D. Tilley, *Organometallics*, 2001, **20**, 5598–5605.

70 D. Martin, J. Kleemann, E. Abinet, T. P. Spaniol, L. Maron and J. Okuda, *Eur. J. Inorg. Chem.*, 2013, 3987.

71 A. Z. Voskoboinikov, I. N. Parshina, A. K. Shestakova, K. P. Butin, I. P. Beletskaya, L. G. Kuz'mina and J. A. K. Howard, *Organometallics*, 1997, **16**, 4041–4055.

72 X. Zhu, D. Guo, Z. Huang, T. Sheng, S. Wang, M. Pan, L. Zha and S. Zhou, *Inorg. Chem.*, 2020, **59**, 14152.

73 W. J. Evans, J. H. Meadows, A. L. Wayda, W. E. Hunter and J. L. Atwood, *J. Am. Chem. Soc.*, 1982, **104**, 2015–2017.

74 D. A. Buschmann, L. Schumacher and R. Anwander, *Chem. Commun.*, 2022, **58**, 9132.

75 E. C. Moinet, O. Tardif, C. Maichle-Mössmer and R. Anwander, *Chem. Commun.*, 2023, **59**, 5261–5264.

76 K. Lv and D. Cui, *Organometallics*, 2010, **29**, 2987–2993.

77 S. Schäfer, S. Kaufmann, E. S. Rösch and P. W. Roesky, *Chem. Soc. Rev.*, 2023, **52**, 4006–4045.

78 D. Schuhknecht, K.-N. Truong, T. P. Spaniol, L. Maron and J. Okuda, *Chem. Commun.*, 2018, **54**, 11280.

79 G. M. Richardson, M. J. Evans, T. Rajeshkumar, J. A. J. McCone, S. A. Cameron, L. Maron, C. Jones and M. D. Anker, *Chem. – Eur. J.*, 2024, **30**(27), e202400681.

80 Y. K. Gun'ko, P. B. Hitchcock and M. F. Lappert, *Organometallics*, 2000, **19**, 2832.

81 D. N. Huh, L. E. Darago, J. W. Ziller and W. J. Evans, *Inorg. Chem.*, 2018, **57**, 2096.

82 W. Huang, F. Dulong, S. I. Khan, T. Cantat and P. L. Diaconescu, *J. Am. Chem. Soc.*, 2014, **136**, 17410–17413.

83 M. E. Fieser, C. T. Palumbo, H. S. L. Pierre, D. P. Halter, V. K. Voora, J. W. Ziller, F. Furche, K. Meyer and W. J. Evans, *Chem. Sci.*, 2017, **8**, 7424.

84 S. P. Nolan and T. J. Marks, *J. Am. Chem. Soc.*, 1989, **111**, 8538–8540.

85 L. Perrin, L. Maron, O. Eisenstein, D. J. Schwartz, C. J. Burns and R. A. Andersen, *Organometallics*, 2003, **22**, 5447–5453.

86 J. Cheng, K. Saliu, G. Y. Kiel, M. J. Ferguson, R. McDonald and J. Takats, *Angew. Chem., Int. Ed.*, 2008, **47**, 4910.

87 Y. Luo and Z. Hou, *J. Phys. Chem. C*, 2008, **112**, 635–638.

88 K. R. McClain, H. Kwon, K. Chakarawet, R. Nabi, J. G. C. Kragskow, N. F. Chilton, R. D. Britt, J. R. Long and B. G. Harvey, *J. Am. Chem. Soc.*, 2023, **145**, 8996–9002.

89 T. Stewart, M. Nishiura, Y. Konno, Z. Hou, G. J. McIntyre and R. Bau, *Inorg. Chim. Acta*, 2010, **363**, 562.

90 P. L. Watson and G. W. Parshall, *Acc. Chem. Res.*, 1985, **18**, 51–56.

91 D. J. Mindiola, *Organometallics*, 2020, **39**, 1135–1138.

92 R. D. Dicken, A. Motta and T. J. Marks, *ACS Catal.*, 2021, **11**, 2715–2734.

93 G. Jeske, H. Lauke, H. Mauermann, P. N. Swepston, H. Schumann and T. J. Marks, *J. Am. Chem. Soc.*, 1985, **107**, 8091–8103.

94 W. J. Evans, J. H. Meadows, A. L. Wayda, W. E. Hunter and J. L. Atwood, *J. Am. Chem. Soc.*, 1982, **104**, 2008–2014.

95 M. Booij, B. J. Deelman, R. Duchateau, D. S. Postma, A. Meetsma and J. H. Teuben, *Organometallics*, 1993, **12**, 3531–3540.

96 K. H. Den Haan, Y. Wielstra and J. H. Teuben, *Organometallics*, 1987, **6**, 2053–2060.

97 R. Waterman, *Organometallics*, 2013, **32**, 7249–7263.

98 T. Ziegler, E. Folga and A. Berces, *J. Am. Chem. Soc.*, 1993, **115**, 636–646.

99 T. Shima and Z. Hou, *Dalton Trans.*, 2010, **39**, 6858.

100 M. E. Thompson, S. M. Baxter, A. R. Bulls, B. J. Burger, M. C. Nolan, B. D. Santarsiero, W. P. Schaefer and J. E. Bercaw, *J. Am. Chem. Soc.*, 1987, **109**, 203–219.

101 X. Zhou and M. Zhu, *J. Organomet. Chem.*, 2002, **647**, 28–49.

102 A. Motta, I. L. Fragalà and T. J. Marks, *Organometallics*, 2006, **25**, 5533–5539.

103 H. Yasuda, in *Lanthanides: Chemistry and Use in Organic Synthesis*, ed. S. Kobayashi, Springer Berlin Heidelberg, Berlin, Heidelberg, 1999, pp. 255–283, DOI: [10.1007/3-540-69801-9\\_7](https://doi.org/10.1007/3-540-69801-9_7).

104 D. Cui, O. Tardif and Z. Hou, *J. Am. Chem. Soc.*, 2004, **126**, 1312.

105 P. Cui, T. P. Spaniol, L. Maron and J. Okuda, *Chem. – Eur. J.*, 2013, **19**, 13437.

106 J. C. Wedal, L. M. Anderson-Sanchez, M. T. Dumas, C. A. Gould, M. J. Beltrán-Leiva, C. Celis-Barros, D. Páez-Hernández, J. W. Ziller, J. R. Long and W. J. Evans, *J. Am. Chem. Soc.*, 2023, **145**, 10730–10742.

107 Q. Wen, T. Rajeshkumar, L. Maron, X. Leng and Y. Chen, *Angew. Chem., Int. Ed.*, 2022, **61**(25), e202200540.

108 W. J. Evans, J. M. Perotti and J. W. Ziller, *Inorg. Chem.*, 2005, **44**, 5820.

109 B. L. L. Réant, S. T. Liddle and D. P. Mills, *Chem. Sci.*, 2020, **11**, 10871–10886.

110 A. Pindwal, K. Yan, S. Patnaik, B. M. Schmidt, A. Ellern, I. I. Slowing, C. Bae and A. D. Sadow, *J. Am. Chem. Soc.*, 2017, **139**, 16862–16874.

111 X. Pan, C. Wu, H. Fang and C. Yan, *Inorg. Chem.*, 2022, **61**, 14288–14296.

112 M. Visseaux and F. Bonnet, *Coord. Chem. Rev.*, 2011, **255**, 374–420.



113 C. Schadle, D. Schadle, K. Eichele and R. Anwander, *Angew. Chem., Int. Ed.*, 2013, **52**, 13238.

114 M. Widemann, F. S. W. Aicher, M. Bonath, K. Eichele, C. Maichle-Mössmer, H. Schubert, P. Sirsch, R. Anwander and L. Wesemann, *Chem. – Eur. J.*, 2022, **28**, e202201032.

115 F. Ortú, *Chem. Rev.*, 2022, **122**, 6040–6116.

116 B. M. Schmidt, A. Pindwal, A. Venkatesh, A. Ellern, A. J. Rossini and A. D. Sadow, *ACS Catal.*, 2019, **9**, 827–838.

117 K. O. Saliu, J. Takats and M. J. Ferguson, *Acta Crystallogr., Sect. E: Struct. Rep. Online*, 2009, **65**, m643–m644.

118 Z. Xu and Z. Lin, *Coord. Chem. Rev.*, 1996, **156**, 139–162.

119 T. V. Fetrow, J. Zgrablik, R. Bhowmick, F. D. Eckstrom, G. Crull, B. Vlaisavljevich and S. R. Daly, *Angew. Chem., Int. Ed.*, 2022, **61**, e202211145.

120 S. Y. Knjazhanskij, B. M. Bulychev, O. K. Kireeva, V. K. Belsky and G. L. Soloveichik, *J. Organomet. Chem.*, 1991, **414**, 11–22.

121 T. Chowdhury, F. Murphy, A. R. Kennedy, C. Wilson, J. H. Farnaby and C. E. Weetman, *Inorg. Chem.*, 2024, **63**(21), 9390–9394.

122 T. Pugh, V. Vieru, L. F. Chibotaru and R. A. Layfield, *Chem. Sci.*, 2016, **7**, 2128–2137.

123 J. Du, P. J. Cobb, J. Ding, D. P. Mills and S. T. Liddle, *Chem. Sci.*, 2024, **15**, 13–45.

124 T. Bauer, F. R. Wagner and R. Kempe, *Chem. – Eur. J.*, 2013, **19**, 8732–8735.

125 M. L. H. Green, A. K. Hughes, D. M. Michaelidou and P. Mountford, *J. Chem. Soc., Chem. Commun.*, 1993, 591–593, DOI: [10.1039/c39930000591](https://doi.org/10.1039/c39930000591).

126 T. Shima and Z. Hou, *Chem. Lett.*, 2008, **37**, 298.

127 A. P. Sobaczynski, T. Bauer and R. Kempe, *Organometallics*, 2013, **32**, 1363.

128 T. Bauer, F. R. Wagner and R. Kempe, *Chem. – Eur. J.*, 2013, **19**, 8732.

129 T. Shima and Z. Hou, *Organometallics*, 2009, **28**, 2244.

130 D. Kawai, T. Shima, M. Nishiura and Z. Hou, *J. Organomet. Chem.*, 2017, **847**, 74.

131 T. Shima, Y. Luo, T. Stewart, R. Bau, G. J. McIntyre, S. A. Mason and Z. Hou, *Nat. Chem.*, 2011, **3**, 814.

132 S. T. Liddle, *Angew. Chem., Int. Ed.*, 2015, **54**, 8604–8641.

133 P. F. Souter, G. P. Kushto, L. Andrews and M. Neurock, *J. Phys. Chem. A*, 1997, **101**, 1287–1291.

134 P. F. Souter, G. P. Kushto, L. Andrews and M. Neurock, *J. Am. Chem. Soc.*, 1997, **119**, 1682–1687.

135 M. Straka and P. Pyykkö, *J. Am. Chem. Soc.*, 2005, **127**, 13090–13091.

136 J. Raab, R. H. Lindh, X. Wang, L. Andrews and L. Gagliardi, *J. Phys. Chem. A*, 2007, **111**, 6383–6387.

137 X. Wang, L. Andrews and L. Gagliardi, *J. Phys. Chem. A*, 2008, **112**, 1754–1761.

138 J. E. Burke and C. S. Smith, *J. Am. Chem. Soc.*, 1947, **69**, 2500–2502.

139 L. Natrajan, M. Mazzanti, J.-P. Bezombes and J. Pécaut, *Inorg. Chem.*, 2005, **44**, 6115–6121.

140 T. Schleid, G. Meyer and L. R. Morss, *J. Less-Common Met.*, 1987, **132**, 69–77.

141 L. Havela, D. Legut and J. Kolorenč, *Rep. Prog. Phys.*, 2023, **86**, 056501.

142 F. Le Guyadec, X. Génin, J. P. Bayle, O. Dugne, A. Duhart-Barone and C. Ablitzer, *J. Nucl. Mater.*, 2010, **396**, 294–302.

143 D. D. Schnaars, G. Wu and T. W. Hayton, *Dalton Trans.*, 2008, 6121–6126, DOI: [10.1039/B809184F](https://doi.org/10.1039/B809184F).

144 J.-C. Berthet, M. Nierlich and M. Ephritikhine, *C. R. Chim.*, 2002, **5**, 81–87.

145 J. Su, E. R. Batista, K. S. Boland, S. E. Bone, J. A. Bradley, S. K. Cary, D. L. Clark, S. D. Conradson, A. S. Ditter, N. Kaltsoyannis, J. M. Keith, A. Kerridge, S. A. Kozimor, M. W. Löble, R. L. Martin, S. G. Minasian, V. Mocko, H. S. La Pierre, G. T. Seidler, D. K. Shuh, M. P. Wilkerson, L. E. Wolfsberg and P. Yang, *J. Am. Chem. Soc.*, 2018, **140**, 17977–17984.

146 J. M. Manriquez, P. J. Fagan and T. J. Marks, *J. Am. Chem. Soc.*, 1978, **100**, 3939–3941.

147 W. J. Evans, K. A. Miller, S. A. Kozimor, J. W. Ziller, A. G. DiPasquale and A. L. Rheingold, *Organometallics*, 2007, **26**, 3568–3576.

148 N. A. Siladke, C. L. Webster, J. R. Walensky, M. K. Takase, J. W. Ziller, D. J. Grant, L. Gagliardi and W. J. Evans, *Organometallics*, 2013, **32**, 6522–6531.

149 W. J. Evans, K. A. Miller, A. G. DiPasquale, A. L. Rheingold, T. J. Stewart and R. Bau, *Angew. Chem., Int. Ed.*, 2008, **47**, 5075–5078.

150 M. Falcone, R. Scopelliti and M. Mazzanti, *J. Am. Chem. Soc.*, 2019, **141**, 9570–9577.

151 R. Chen, G. Qin, S. Li, A. J. Edwards, R. O. Piltz, I. Del Rosal, L. Maron, D. Cui and J. Cheng, *Angew. Chem., Int. Ed.*, 2020, **59**, 11250–11255.

152 G. Qin, Y. Wang, X. Shi, I. Del Rosal, L. Maron and J. Cheng, *Chem. Commun.*, 2019, **55**, 8560–8563.

153 M. Falcone, L. N. Poon, F. Fadaei Tirani and M. Mazzanti, *Angew. Chem., Int. Ed.*, 2018, **57**, 3697–3700.

154 C. T. Palumbo, R. Scopelliti, I. Zivkovic and M. Mazzanti, *J. Am. Chem. Soc.*, 2020, **142**, 3149–3157.

155 C. T. Palumbo, L. Barluzzi, R. Scopelliti, I. Zivkovic, A. Fabrizio, C. Corminboeuf and M. Mazzanti, *Chem. Sci.*, 2019, **10**, 8840–8849.

156 D.-D. Zhai, H.-Z. Du, X.-Y. Zhang, Y.-F. Liu and B.-T. Guan, *ACS Catal.*, 2019, **9**, 8766–8771.

157 J.-C. Berthet, J.-F. Le Maréchal and M. Ephritikhine, *J. Chem. Soc., Chem. Commun.*, 1991, 360–361, DOI: [10.1039/C39910000360](https://doi.org/10.1039/C39910000360).

158 J.-F. Le Maréchal, C. Villiers, P. Charpin, M. Lance, M. Nierlich, J. Vigner and M. Ephritikhine, *J. Chem. Soc., Chem. Commun.*, 1989, 308–310, DOI: [10.1039/C39890000308](https://doi.org/10.1039/C39890000308).

159 J.-C. Berthet, C. Villiers, J.-F. Le Maréchal, B. Delavaux-Nicot, M. Lance, M. Nierlich, J. Vigner and M. Ephritikhine, *J. Organomet. Chem.*, 1992, **440**, 53–65.

160 M. R. MacDonald, M. E. Fieser, J. E. Bates, J. W. Ziller, F. Furche and W. J. Evans, *J. Am. Chem. Soc.*, 2013, **135**, 13310–13313.



161 W. Ren, N. Zhao, L. Chen, H. Song and G. Zi, *Inorg. Chem. Commun.*, 2011, **14**, 1838–1841.

162 J. K. Pagano, J. M. Dorhout, R. Waterman, K. R. Czerwinski and J. L. Kiplinger, *Chem. Commun.*, 2015, **51**, 17379–17381.

163 R. R. Langeslay, M. E. Fieser, J. W. Ziller, F. Furche and W. J. Evans, *J. Am. Chem. Soc.*, 2016, **138**, 4036–4045.

164 C. J. Windorff, M. R. MacDonald, K. R. Meihaus, J. W. Ziller, J. R. Long and W. J. Evans, *Chem. – Eur. J.*, 2016, **22**, 772–782.

165 R. W. Broach, A. J. Schultz, J. M. Williams, G. M. Brown, J. M. Manriquez, P. J. Fagan and T. J. Marks, *Science*, 1979, **203**, 172–174.

166 Z.-L. Xue, T. M. Cook and A. C. Lamb, *J. Organomet. Chem.*, 2017, **852**, 74–93.

167 C. M. Fendrick, L. D. Schertz, V. W. Day and T. J. Marks, *Organometallics*, 1988, **7**, 1828–1838.

168 W. J. Evans, K. A. Miller and J. W. Ziller, *Angew. Chem., Int. Ed.*, 2008, **47**, 589–592.

169 W. J. Evans, G. W. Nyce and J. W. Ziller, *Organometallics*, 2001, **20**, 5489–5491.

170 E. Zhou, W. Ren, G. Zi, D.-C. Fang and M. D. Walter, *Organometallics*, 2015, **34**, 3637–3647.

171 W. Ren, E. Zhou, B. Fang, G. Zi, D.-C. Fang and M. D. Walter, *Chem. Sci.*, 2014, **5**, 3165–3172.

172 R. A. Andersen, A. Zalkin and D. H. Templeton, *Inorg. Chem.*, 1981, **20**, 622–623.

173 D. L. Clark, S. K. Grumbine, B. L. Scott and J. G. Watkin, *J. Am. Chem. Soc.*, 1995, **117**, 9089–9090.

174 D. L. Clark, S. K. Grumbine, B. L. Scott and J. G. Watkin, *Organometallics*, 1996, **15**, 949–957.

175 H. S. La Pierre, H. Kameo, D. P. Halter, F. W. Heinemann and K. Meyer, *Angew. Chem., Int. Ed.*, 2014, **53**, 7154–7157.

176 J. A. Higgins, F. G. N. Cloke and S. M. Roe, *Organometallics*, 2013, **32**, 5244–5252.

177 M. R. Duttera, P. J. Fagan, T. J. Marks and V. W. Day, *J. Am. Chem. Soc.*, 1982, **104**, 865–867.

178 J.-C. Berthet, J.-F. Le Maréchal, M. Lance, M. Nierlich, J. Vigner and M. Ephritikhine, *J. Chem. Soc., Dalton Trans.*, 1992, 1573–1577, DOI: [10.1039/DT9920001573](https://doi.org/10.1039/DT9920001573).

179 K. Li, I. Del Rosal, Y. Zhao, L. Maron and C. Zhu, *Angew. Chem., Int. Ed.*, 2024, e202405494, DOI: [10.1002/anie.202405494](https://doi.org/10.1002/anie.202405494).

180 P. Hrobarik, V. Hrobarikova, A. H. Greif and M. Kaupp, *Angew. Chem., Int. Ed.*, 2012, **51**, 10884–10888.

181 H. W. Turner, S. J. Simpson and R. A. Andersen, *J. Am. Chem. Soc.*, 1979, **101**, 2782–2782.

182 S. J. Simpson, H. W. Turner and R. A. Andersen, *Inorg. Chem.*, 1981, **20**, 2991.

183 A. K. Dash, J. Q. Wang and M. S. Eisen, *Organometallics*, 1999, **18**, 4724–4741.

184 N. Tsoureas, L. Maron, A. F. R. Kilpatrick, R. A. Layfield and F. G. N. Cloke, *J. Am. Chem. Soc.*, 2020, **142**, 89–92.

185 I. J. Brackbill, T. Rajeshkumar, L. Maron, R. G. Bergman and J. Arnold, *J. Am. Chem. Soc.*, 2024, **146**(2), 1257–1261.

186 T. J. Marks and J. R. Kolb, *Chem. Rev.*, 1977, **77**, 263–293.

187 P. L. Arnold, J. H. Farnaby, M. G. Gardiner and J. B. Love, *Organometallics*, 2015, **34**, 2114–2117.

188 P. L. Arnold, C. J. Stevens, J. H. Farnaby, M. G. Gardiner, G. S. Nichol and J. B. Love, *J. Am. Chem. Soc.*, 2014, **136**, 10218–10221.

189 N. Tsoureas, A. Mansikkamäki and R. A. Layfield, *Chem. Commun.*, 2020, **56**, 944–947.

190 J. T. Boronski, L. R. Doyle, J. A. Seed, A. J. Woole and S. T. Liddle, *Angew. Chem., Int. Ed.*, 2020, **59**, 295–299.

191 D. Baudry, E. Bulot, P. Charpin, M. Ephritikhine, M. Lance, M. Nierlich and J. Vigner, *J. Organomet. Chem.*, 1989, **371**, 155–162.

192 R. R. Ryan, K. V. Salazar, N. N. Sauer and J. M. Ritchey, *Inorg. Chim. Acta*, 1989, **162**, 221–225.

193 D. Männig and H. Nöth, *Z. Anorg. Allg. Chem.*, 1986, **543**, 66–72.

194 A. C. Dunbar, J. C. Wright, D. J. Grant and G. S. Girolami, *Inorg. Chem.*, 2021, **60**, 12489–12497.

195 R. H. Banks, N. M. Edelstein, R. R. Rietz, D. H. Templeton and A. Zalkin, *J. Am. Chem. Soc.*, 1978, **100**, 1957–1958.

196 H. R. Hoekstra and J. J. Katz, *J. Am. Chem. Soc.*, 1949, **71**, 2488–2492.

197 T. V. Fetrow, J. P. Grabow, J. Leddy and S. R. Daly, *Inorg. Chem.*, 2021, **60**, 7593–7601.

198 L. Maria, I. C. Santos and I. Santos, *Dalton Trans.*, 2018, **47**, 10601–10612.

199 A. Dauth and J. A. Love, *Dalton Trans.*, 2012, **41**, 7782–7791.

200 A. B. Altman, A. C. Brown, G. Rao, T. D. Lohrey, R. D. Britt, L. Maron, S. G. Minasian, D. K. Shuh and J. Arnold, *Chem. Sci.*, 2018, **9**, 4317–4324.

201 C. Z. Ye, I. Del Rosal, M. A. Boreen, E. T. Ouellette, D. R. Russo, L. Maron, J. Arnold and C. Camp, *Chem. Sci.*, 2023, **14**, 861–868.

